ORIGINAL ARTICLE





Thermochemical principles of the production of lightweight aggregates from waste coal bottom ash

Mohammad Balapour¹ | Rathin Rao² | Edward J. Garboczi³ | Sabrina Spatari¹ | Y. Grace Hsuan¹ | Pieter Billen⁴ | Yaghoob Farnam¹

Correspondence

Mohammad Balapour, Drexel University, Department of Civil, Architectural and Environmental Engineering, 3141 Chestnut Street, Philadelphia, PA 19104, USA. Email: Mohammad.balapour@drexel.edu

Funding information

National Science foundation (NSF), Grant/ Award Number: CMMI - 1550723 and PFI-TT 1918838

Abstract

Manufacturing lightweight aggregate (LWA) (ie, porous ceramics) by means of a sintering technique requires a delicate balance among three conditions: (a) forming a sufficient amount of molten liquid phase during sintering, (b) reaching an appropriate viscosity for solid-liquid suspension, and (c) emitting a sufficient amount of gas that can be entrapped by the liquid phase to form pores. This study evaluates these three conditions in the production of LWAs made from two types of waste coal bottom ash (low-calcium and high-calcium), and relates them to the formation of LWA pore structure. A thermochemical analytical approach, including thermodynamic modeling and the Browning viscosity model, was used to quantify the extent of the liquid phase and calculate its viscosity. In conjunction with thermochemical analysis, an experimental approach including quantitative x-ray diffractometry, thermogravimetric analysis, and x-ray computed tomography was also used to identify the candidate chemical compounds that contribute to gas emission during sintering and to evaluate the LWA pore structure. The results indicated that a mass fraction of at least 50% for the liquid phase is required for a successful entrapment of emitted gaseous phases during sintering. Larger pores were observed in the microstructure of LWA samples made using high-calcium bottom ash in comparison to those made with low-calcium bottom ash. This observation was mainly attributed to the high-calcium samples forming liquid phases with lower viscosities and emitting higher amounts of gaseous phase during sintering than did the low-calcium samples. It was found that the gaseous phase was generated by hematite reduction and anhydrite decomposition, which led to the release of O_2 and SO_2 .

KEYWORDS

bottom ash, coal combustion product, gaseous phase, lightweight aggregate, liquid phase, sintering, viscosity

1 INTRODUCTION

Bottom ash is a type of Coal Combustion Product (CCP) and is currently considered to be a waste material needing to be landfilled. In 2017, nearly 10 billion kg of bottom ash were produced from which only $\approx 50\%$ was recycled. Landfilling

of unused bottom ash can impose a risk to the environment and human health.^{2,3} Accordingly, new regulations made by the United States Environmental Protection Agency (EPA)⁴ encourage new methodologies to convert CCPs into valueadded products. Producing functional lightweight aggregate (LWA) for the construction industry from bottom ash can be

¹Department of Civil, Architectural and Environmental Engineering, Drexel University, Philadelphia, PA, USA

²Department of Mechanical Engineering and Mechanics, Drexel University, Philadelphia, PA, USA

³Applied Chemicals and Materials Division, National Institute of Standards and Technology, Boulder, CO, USA

⁴University of Antwerp, Antwerp, Belgium

a practical approach to help landfill diversion and recycling waste CCPs. Sintering is one of the techniques that can be employed in order to produce LWA from CCPs. However, successful production of LWA from CCPs requires an advanced understanding of the sintering mechanisms taking place during the production process.

Previous studies of LWA production from various starting waste materials⁵⁻¹¹ have suggested that a successful production of sintered LWA requires a sintering mechanism where three crucial conditions are reached concurrently during sintering^{7,12}: (a) sufficient liquid/molten phase amount formation on the aggregate surface to maintain a viscous state for the LWA, (b) attaining an appropriate viscosity in the liquid-solid suspension to enable the entrapment emitted gas during sintering while preventing extreme LWA deformations under gravitational forces, and (c) appropriate amount of gaseous phase emission during sintering to form entrapped pores in the liquid phase that will result in successful bloating and LWA formation. Providing a balance among these three conditions can lead to successful design and production of functional LWA having desirable engineering properties for different industrial applications. Some of the applications are internal curing of concrete,⁵ lightweight concrete, lightweight fill for geotechnical applications, wastewater treatment, 13 and green roofs. For applications such as internal curing of concrete and green roofs, the desirable engineering properties are interconnected pores with appropriate porosity (>20% by volume) as well as appropriate water absorption/desorption properties (water absorption >5% and minimum of 85% water desorption at 94% relative humidity^{5,14}). In the case of using LWA in lightweight concrete and lightweight fill for geotechnical applications, the bulk density and compressive strength are the important engineering properties, and the recommended values are 650-1100 kg/m³ and about 2 MPa, respectively, ^{15,16} For application in wastewater treatment, the pore structure and the ability to retain contaminants are the designing parameters. ¹⁷ Figure 1 shows a schematic representation of a typical synthetic LWA, with development of a core and shell structure morphology after sintering.¹⁸

1.1 | Background on conditions for sintering

1.1.1 | Formation of liquid phase during sintering

During LWA production through sintering, formation of a liquid phase favors the integrity of the LWA and provides strength. ¹⁹ As a viscous medium, it captures emitted gas to form pores in the LWA (Figure 1). Lack of a sufficient amount of liquid phase not only prevents entrapment of the gaseous phase as pores, but also leads to poor LWA

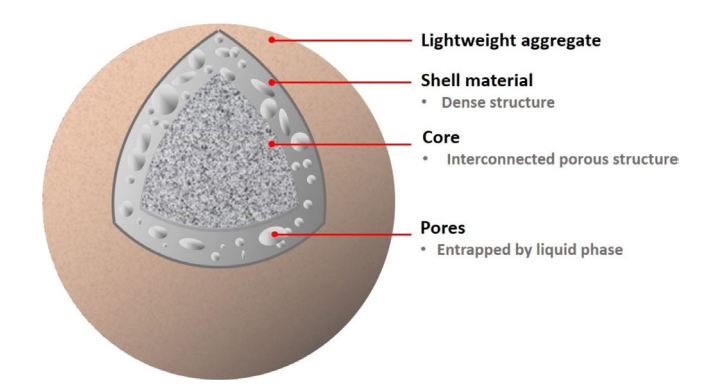


FIGURE 1 Schematic representation of a synthetic lightweight aggregate with core and shell morphology^{7,18}

compressive strength due to inadequate particle bonding. To quantify the mass of liquid phase formed when waste coal ash is sintered, thermodynamic modeling can be used to predict the formation of the most stable phases (including the liquid phase) from the sintered materials with different chemical compositions. ^{12,19,20} The presence of more than 50% of liquid phase (by total mass of feed materials) has been shown to be necessary for production of high-quality LWA. ²⁰ It has been also reported that an excessive amount of high viscosity liquid phase can result in pore sealing and reduction in sorption properties for the resulting LWA. ^{10,21}

1.1.2 | Viscosity of liquid phase

Viscosity of the solid-liquid suspension during sintering is another crucial condition for LWA design and production. Low viscosity values cannot only lead to considerable deformation and collapse of the molten phase but also result in eruption of the emitted gaseous phase and generation of overly-large pores in LWA. The right viscosity can ensure stable entrapment of the gaseous phase leading to successful bloating behavior, forming a desirable LWA pore system. The dynamics of gas-filled pore growth, which determines the final pore size, in a viscous medium is highly dependent on the liquid phase viscosity. It has been shown that the viscosity of the liquid phase is mainly dependent on its chemical composition 12,23,24 and can be predicted using empirical models such as those of Browning 44 and Urbain. 25

Few studies have quantified the viscosity of the solid-liquid phase in LWA production. Billen et al¹² investigated the production of lightweight melt ceramics from bottom ash using NaOH as a fluxing agent to promote melting behavior so as to entrap emitted gaseous phases at sintering temperatures near 1160°C. Their results showed that for production of lightweight melt ceramics, without any deformation under gravitational forces, the solid-liquid suspension should have a viscosity >1000 Pa·s.

1.1.3 | Formation of gaseous phase

Liberation of an appropriate amount of gaseous phase is crucial for LWA production. The addition of hematite, pyrite, dolomite and calcite to non-bloating clays can lead to good bloating behavior for clay-based LWA.²³ However, calcite was not found to be a promising bloating agent for LWA production since its addition produces a low viscosity molten phase and results in overly-large pores and excessive deformation in the final LWA product.²³ Rincón et al²⁶ reported that for successful production of a glass-based LWA, possessing high permeability and low density, there should be a delicate balance between viscous flow sintering and gas emission. They stated that gas emission can happen through oxidation and decomposition reactions at elevated temperatures where oxidation reactions involve release of CO_{x (x=1,2)} gas from carbon-containing compounds and decomposition originates from carbonates or sulfates emitting CO₂ or SO₃ gases. Another type of decomposition can arise from reduction of metal oxides transforming from high valence states into low valence states, which leads to oxygen gas release. 27,28 Reduction of hematite (Fe₂O₂) and emission of oxygen during the sintering process has been proposed by researchers as a source of gas release for pore formation (Equations 1 and 2).²⁶ It has been found that the extent of this reduction is dependent on the unburnt carbon content available in the system.²⁹ Reduction in hematite highly depends on the partial pressure of oxygen. At 0.101 MPa (1 atm), this reduction happens at 1400°C, which is significantly higher than the temperature at which a liquid phase forms on the surface of a typical LWA (ie, 1100-1200°C). 30 By decreasing the oxygen partial pressure, however, reduction of hematite can shift to 1100°C. This can be achieved by rapid sintering where the surface of LWA quickly turns into liquid phase and seals the entire LWA, and oxygen partial pressure decreases by carbon burning inside the LWA resulting in the reduction in hematite and the release of O₂ gas.³¹

$$6Fe_2O_3(s) \rightarrow 4Fe_3O_4(s) + O_2(g)$$
 (1)

$$2\text{Fe}_3\text{O}_4(s) \to 6\text{FeO}(s) + \text{O}_2(g)$$
 (2)

Wei and Lin¹¹ investigated the role of Fe compounds on LWA production from reservoir sediments containing silicate-alumina-based materials.³² The material was dried and then ground to fine particles, and finally were shaped into pellets by applying 34.5 MPa (5000 psi) pressure. The sintering was carried out at 1050°C and 1150°C. They observed that the bloating mechanism occurred at the core of the LWA that was sintered at 1150°C and was associated with the release of SO₂, SO₃ and O₂ gases due to the decomposition of FeSO₄. Wei et al³³ investigated the effect of calcium compounds, including calcite and gypsum (CaSO₄.2H₂O) additions, as

bloating agents on LWA pore formation in coal fly ash mixed with waste glass. Their thermogravimetric analysis (TGA) results on pure calcite demonstrated a rapid mass loss from 600°C to 780°C and relatively no mass loss from 780°C to 1200°C. For gypsum, they observed a rapid decomposition starting at 100°C and ending at 160°C related to the release of water from the gypsum structure. The mass loss from 160°C to 1100°C was negligible for gypsum. However, decomposition between 1100°C and 1200°C was observed and was associated with the decomposition of CaSO₄ to CaO and the release of SO₂ gas. 34

Previous works have described successful production of a novel LWA, spherical porous reactive lightweight aggregate (SPoRA), from high-calcium and low-calcium bottom ash, 10,12 where the functionality of these LWA for internal curing of concrete was found to be promising.⁵ This paper builds on these previous results to better understand the SPoRA sintering mechanisms by quantitatively evaluating the three crucial sintering conditions required for successful production of LWA: the correct amount of liquid phase formation, the correct viscosity of the liquid-solid suspension, and the correct amount of the emitted gas for pore formation. First, the liquid phase of the multi-component system of bottom ash and fluxing agent was quantified using thermodynamic modeling. Second, the viscosity of the liquid-solid phase was quantified using the output of thermodynamic modeling as inputs into the Browning and Krieger-Dougherty model equations.^{24,35,36} Third, quantitative x-ray diffractometry (QXRD) and TGA were performed to assess the presence of the candidate chemical compounds that can lead to gas liberation during sintering and to understand the thermal behavior of geopolymerized (ie, experienced/underwent the chemical rection between the dissolved species of aluminates and silicates in a highly alkaline environment to form a three-dimensional aluminosilicate network³⁷) pellets during sintering. Finally, the interior physical features and the LWA pore structure were visualized using three-dimensional (3D) x-ray computed tomography (X-CT).

2 | MATERIALS AND RESEARCH METHODOLOGY

2.1 Materials

Two types of bottom ash, NV (low-calcium) and WP (high-calcium), were used in this study for LWA production.^{5,12} The LWA manufacturing procedure started by drying the raw ash material, followed by sieving to the appropriate particle size distribution. Afterward, the prepared ash was mixed with various NaOH solutions (molarities of 2.5, 6.25, and 10 mol/L) to achieve mass concentrations (mass of solid NaOH per mass of bottom ash) of 4%, 10%, and

16%. NaOH solutions with a liquid to solid ratio of 0.4 were used for geopolymerization during the curing period as well as to serve as a fluxing agent to reduce the melting temperature of the mixture. ^{5,12} The mixture was then pelletized into spherical shape and cured at 40°C and 30% relative humidity (RH) for 24 hours. Finally, the pellets were sintered at 1160°C to produce SPoRA. The detailed SPoRA manufacturing process can be found elsewhere. ^{5,12} Samples were labeled as XX-YY%, where XX represents the bottom ash type (NV or WP), while YY% indicates the NaOH concentration.

2.2 | Research methodology

The research methodology was divided into two parts, analytical modeling and experimental investigation, to examine the required conditions for LWA production. The analytical part employed thermodynamic modeling and viscosity calculations to quantify liquid phase formation as a function of temperature during sintering and to calculate viscosity values for the resulting solid-liquid suspension. Experiments were used to study the chemical compounds that can lead to gas emission during the sintering process and quantify the amount of the emitted gaseous phase that leads to LWA pore formation. The pore-solid structure of LWA was investigated using X-CT with respect to the three conditions required for successful LWA production.

2.2.1 | Analytical modeling

The analytical modeling in this study was built on the previous work conducted by Billen et al¹² to understand the thermodynamic response and fluid behavior of solid-liquid suspension during sintering. Analytical modeling consisted of developing phase equilibria and quantification of liquid phase formation using the Factsage* software^{38,39} as well as using the thermodynamic modeling outputs, including the chemical composition of the liquid phase, to calculate the viscosity of solid-liquid system.

Factsage simulation

The Factsage thermodynamic modeling software, along with the FToxide database, 40 were used to predict multi-phase equilibria based on Gibbs' free energy minimization algorithm for the multi-component system during sintering. 19,41 The simulation was performed at 0.101 MPa (1 atm) under an ordinary air atmosphere, which was composed of 0.21 mole fraction oxygen and 0.79 mole fraction nitrogen, in accordance with the conditions of LWA sintering. The initial and final temperatures for the modeling were set to 800°C and 1400°C, respectively, with 50°C intervals. The major chemical oxides of the ashes, which were used as the input in the Factsage software, were determined using x-ray fluorescence (XRF) and are presented in Table 1. 5,12 In addition, NaOH was used as the fluxing agent in the thermodynamic modeling.

Viscosity calculations

Empirical models have been developed to predict coal ash liquid phase (slag) viscosity based on a simplified slag chemical composition. 25,43-45 The empirical model developed by Browning et al²⁴ was found to be more applicable for the prediction of the liquid phase (slag) viscosity ¹² due to experimentally determined lower bias and higher accuracy compared with earlier developed models such as those of Watt and Fereday⁴⁴ and Urbain.²⁵ The Browning model assumes that the viscosity of the slag falls into a Newtonian region⁴⁶ and correlates viscosity with temperature (T) using a temperature shift (T_s) (Equation 3). T_s, as presented in Equation 4, is a function of a composition parameter, ie, A. A is defined as the weighted molar ratio of network formers (numerator of Equation 5) to network modifiers (denominator of Equation 5) elements as presented in Equation 5, where the quantity of each component is in mole fraction and their summation must add up to unity (Equation 6).

$$\log_{10}\left(\frac{\eta_L}{T - T_s}\right) = \frac{14788}{T - T_s} - 10.931\tag{3}$$

$$T_s = 306.63. \ln(A) - 574.31$$
 (4)

$$A = \frac{3.19 \text{Si}^{4+} + 0.855 \text{AI}^{3+} + 1.6 \text{K}^{+}}{0.93 \text{Ca}^{2+} + 1.50 \text{Fe}^{n+} + 1.21 \text{Mg}^{2+} + 0.69 \text{Na}^{+} + 1.35 \text{Mn}^{n+} + 1.47 \text{Ti}^{4+} + 1.91 \text{S}^{2-}}$$
(5)

$$Si^{4+} + Al^{3+} + Ca^{2+} + Fe^{n+} + Mg^{2+} + Na^{+} + K^{+} + Mn^{n+} + Ti^{4+} + S^{2-} = 1$$
(6)

The composition of the liquid phase (slag) at different temperatures for each LWA was obtained using Factsage with varying fluxing agent concentrations and was used to estimate the viscosity

^{*}Certain commercial equipment, software and/or materials are identified in this paper in order to adequately specify the experimental procedure. In no case does such identification imply recommendation or endorsement by the National Institute of Standards and Technology, nor does it imply that the equipment and/or materials used are necessarily the best available for the purpose.

TABLE 1 Major chemical oxide compositions of NV and WP ashes used in this study

	Sample Name	
Chemical composition (% by mass)	NV	WP
SiO_2	63.2	43.1
Al_2O_3	20.1	17.1
Fe_2O_3	6.66	7.29
CaO	3.51	22.5
Na_2O	1.43	1.19
MgO	0.97	4.10
Total	95.89	95.31

TABLE 2 Experimental program

Experimental investigation

2.2.2

Quantitative x-ray powder diffraction (OXRD)

techniques used to study each part.

X-ray diffraction analysis was performed using a Rigaku Smartlab instrument using steps of 0.02° in a 10° to 70°

structure of the final SPoRA product. Table 2 summarizes the

Part	Test	Purpose
(1): Raw Material Acquisition	XRF	To assess the chemical composition of ashes (discussed in Viscosity calculation and conducted by the bottom ash provider)
	QXRD	To quantify the mineral phases of ashes
	TGA	To determine the free carbon content of ashes
(2): Geopolymerization	QXRD	To assess formation of new mineral phases at different concentrations of NaOH in the geopolymerized pellets
(3): Sintering	TGA	To identify the candidate reactions and products that contribute to the formation of pores
(4): Final product	X-CT	To assess internal morphological features and the SPoRA pore structure

of the liquid phase. It should be noted that during sintering at some temperatures, the LWA system is composed of liquid and solid phase concurrently; therefore, the suspension's (solid-liquid phase) viscosity becomes highly dependent on the volume fraction of solid phase. Thus, to estimate the viscosity of solid-liquid suspension, the Krieger and Dougherty model⁴⁷ was used (Equation 7).

$$\eta_{s} = \eta_{L} \left(1 - \frac{\phi}{\phi_{m}} \right)^{-[\eta]\phi_{m}} \tag{7}$$

where η_s is the viscosity of the liquid-solid suspension, η_I is the liquid phase (slag) viscosity, ϕ is the volume fraction of solids, ϕ_m is the maximum particle packing fraction, and is the volume fraction of solids, ϕ_m is the intrinsic viscosity. This equation is applicable in the range of $[\eta]$. In this study, it was assumed that particles are spheres leading to $0 < \phi < \phi_m$, and $[\eta] = 2.5$ was calculated according to Stovall et al⁴⁸ model and was estimated to be 0.834. The densities of the solid and liquid phases are similar, so that this assumption is accurate to within a few percent. The Krieger and Dougherty model will reduce to the Einstein equation 35,36,49 at ϕ_m , which is associated with the dilute limit considered in Einstein's equation.

 2ϕ < 0.02 range. A Cu_{Kα} source operating at 40 kV and 40 mA was used during the test. Phase identifications and Rietveld refinements were performed using the open source Profex software.⁵⁰

To perform QXRD on the raw materials, the following procedure was adopted: (a) raw NV and WP ashes (with a particle size distribution described in Ref. [5]) were taken separately, (b) the powder was crushed using a mortar and pestle, (c) the obtained powder was sieved through an ASTM #200 sieve (75 µm mesh opening), (d) the portion of powder that was retained on the #200 sieve was re-crushed and sieved to make sure the entire powder passed through the #200 sieve, (e) $0.8 \text{ g} \pm 0.001 \text{ g}$ of the prepared powder was blended with 0.2 g \pm 0.001 g of Rutile (TiO₂), used as a reference powder with purity greater than 99% and mean particle size of 5 µm, and (f) the final blended powder was used in the QXRD test. The same sample preparation procedure was used to prepare QXRD samples of geopolymerized pellets after curing in an environmental chamber at 40°C and 30% RH for 24 hours.

Thermogravimetric analysis (TGA)

TGA was carried out using a TA Instrument Q5000 IR model. To determine the unburned carbon content of the raw material, a 2-atmosphere TGA (2A-TGA) procedure using nitrogen and air gases adopted from Ref. [29] was performed according to Figure 2. This was mainly to separate the oxidization of carbon from other decomposition reactions occurring in the same range of temperatures. In this regard, temperature was increased to 100°C and was kept there for 5 minutes under nitrogen atmosphere in order to evaporate the free water. Next, still under nitrogen gas, the temperature was increased to 750°C with a ramp of 20°C/min. Afterward, under nitrogen gas, the temperature was decreased back to 100°C with a ramp of 20°C/min. In the next step, the gas was changed to air and temperature was kept at 100°C for 5 minutes. Finally, under air, the temperature was increased to 1000°C with a ramp of 20°C/min. Raw materials were crushed using a mortar and pestle and were sieved through a #200 sieve. Crushing and sieving was repeated to ensure that the entire amount of the initial powder had a size smaller than 75 µm. Sample masses of 30 to 40 mg were used in the TGA tests. Considering the melting behavior of LWA at sintering temperature near 1160°C, a fine crucible refractory ceramic powder was used as a bed in the TGA pan to prevent any sintered material adhering to the crucible pan during melting.

For geopolymerized pellets, the same sample preparation procedure was adopted; however, TGA tests were performed under an air atmosphere only to simulate the actual sintering conditions in LWA production. Samples were heated at a rate of 10°C/min to 1160°C (the sintering temperature) and then were held at this temperature for 4 minutes.

X-ray computed tomography (X-CT)

X-CT was performed to non-destructively assess the LWA internal morphology. In this method, a series of projection images of the sample, which is mounted on a rotating stage, were collected. Using tomographic reconstruction, cross-sectional 2D slices were then obtained. ⁵¹⁻⁵³ Three-dimensional sample visualization was obtained by vertically stacking the 2D slices. The X-CT was carried out using a Zeiss Versa XRM 500 system. ⁵ The x-ray tube was set for a voltage of 80 kV and a current of 87 mA. The exposure time per step for 360° rotation was ≈ 0.6 second. The images were taken with a voxel size of approximately 18 μ m. For constructing 3D images, visualizing 2D slices, and videos, the Dragonfly software ⁵⁴ was used.

3 | RESULTS

This section discusses the results of thermodynamic predictions to quantify the liquid phase and its viscosity formed during sintering. The QXRD and the TGA/DTG results are also presented to assess the phase development before sintering and identify the potential compounds that could contribute to gas emission

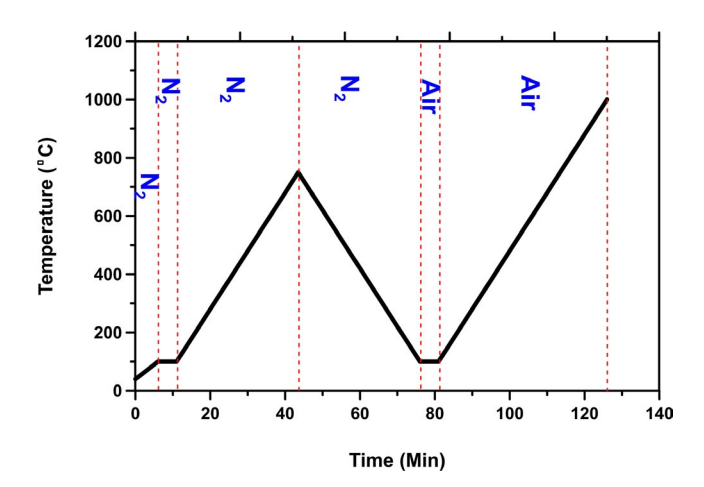


FIGURE 2 2-atmosphere thermogravimetric analysis (2A-TGA) applied for determination of unburnt carbon content of raw materials

during sintering and consequently pore creation. Furthermore, the LWA pore structure was assessed using X-CT.

3.1 | Thermodynamic predictions of LWA multi-component system during sintering

3.1.1 | Phase equilibria and quantification of liquid phase formation

Figure 3 (left column) shows the predicted phase diagrams for NV ash with 0%, 4%, 10%, and 16% addition of NaOH as the fluxing agent. NaOH has three main effects on the sintering process according to thermodynamic modeling: (a) reducing the LWA melting temperature (ash + NaOH), (b) reducing the liquid phase viscosity (since Na⁺ is a network modifier), and (c) initiating geopolymerization for the LWA (ash + NaOH) system. Thermodynamic modeling calculates equilibrium conditions only and does not consider any kinetics governing the sintering process, which may influence the quantity and the type of formed phases. For example, formation of a viscous liquid phase near the LWA surface may hinder the penetration of oxygen to the LWA inner core (discussed in Section 3.5), which can result in a reduction in atmospheric pressure in the outer area and alter the kinetics of phase formation phenomena.

A good quality LWA requires enough liquid phase (slag) to entrap emitted gas near the sintering temperature (1160°C). The slag contents for NV-0%, NV-4%, NV-10%, and NV-16% at 1160°C were estimated to be 2.6%, 47.2%, 59.5%, and 97.8%, respectively. Figure 3 (right column) shows the predicted phase diagrams for WP ash with 0%, 4%, 10%, and 16% addition of NaOH. The slag content for WP-0%, WP-4%, WP-10%, and WP-16% at 1160°C were estimated to be 10.3%, 58.3%, 65.3%, and 85.5%, respectively.

WP-0% had a lower initial melting temperature (ie, 1100°C) compared with NV-0% (ie, 1150°C). This can be

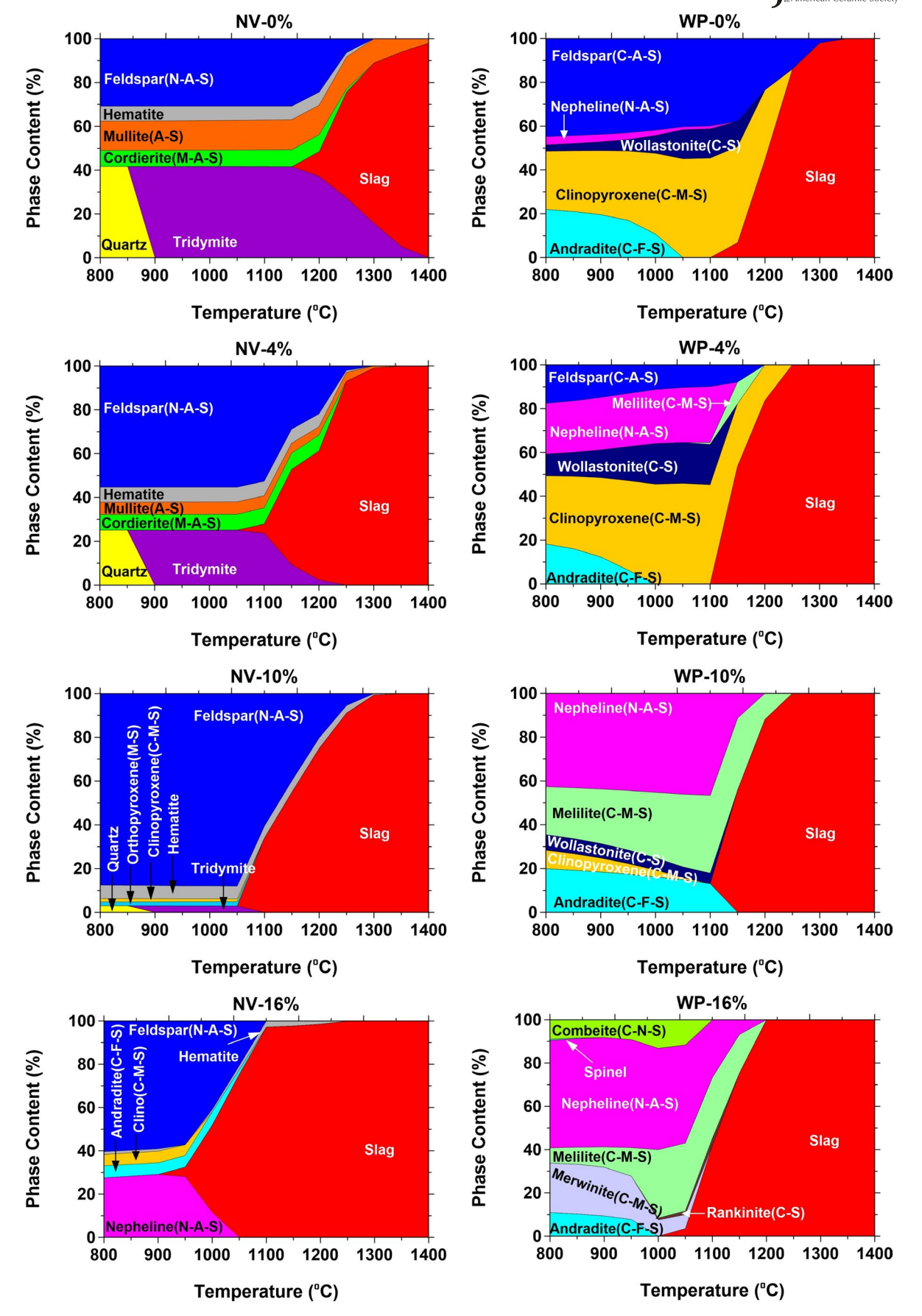


FIGURE 3 Predicted phase diagrams for bottom ash with NaOH concentrations of 0%, 4%, 10%, and 16%: NV bottom ash (left column) and WP bottom ash (right column); C: CaO, A: Al₂O₃, N: Na₂O, S: SiO₂, M: MgO, F: Fe₂O₃

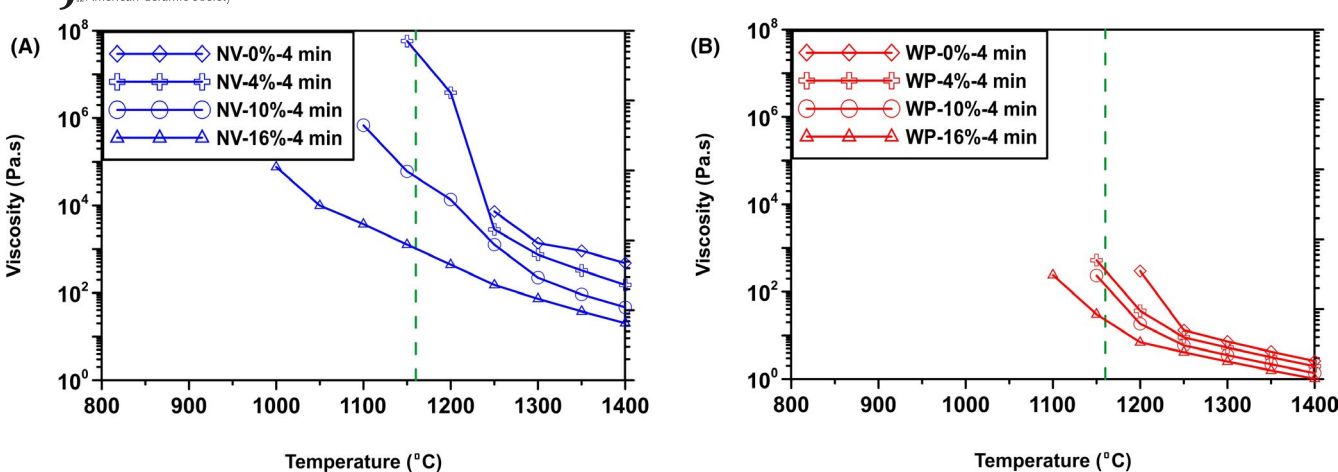


FIGURE 4 Viscosity calculations of solid-liquid system with different NaOH concentration for (A) NV ash and (B) WP ash (the green dashed lines show the furnace operating temperature, 1160°C)

justified by the fact that in a system without NaOH and major presence of SiO₂-Al₂O₃ compounds, increasing the amount of CaO lowers the melting temperature for the CaO-SiO₂-Al₂O₃ system due to the formation of compounds that have lower melting temperature than that of mullite (3Al₂O₃.2SiO₂) formed in a binary system of Al₂O₃ and SiO₂.^{55,56} For NV ash, incorporation of a higher amount of NaOH led to the formation of higher Na-bearing Feldspar (NaAlSi₃O₈) content (as can be seen in the phase diagram), which has a melting temperature close to 1100°C.⁵⁵ Therefore, the melting temperature of NV ash was reduced by increasing the NaOH concentration and higher liquid phase (slag) content was formed. The initial melting temperatures for NV-4%, NV-10%, and NV-16% were 1050°C, 1050°C, and 900°C, respectively.

Addition of NaOH to WP ash did not significantly change the melting temperature for the system (Figure 3 (right column)). This can be explained by the formation of several Ca-bearing phases at elevated temperature in the WP geopolymerized pellets (NaOH added) that have high melting temperatures along with Nepheline (NaAlSiO₄), which has a melting temperature between 1100°C and 1256°C . Accordingly, the melting temperature of the WP-NaOH system remained higher compared to the NV + NaOH system. The melting temperatures for WP-4%, WP-10%, and WP-16% were predicted to be 1100°C , 1100°C , and 1000°C , respectively. It should be noted that formation of Na-bearing phases such as Nepheline (at major quantities) in the WP-NaOH system helped to increase the liquid phase content.

3.1.2 | Viscosity prediction for solidliquid system

Figure 4 shows the estimated viscosity values for solid-liquid systems as a function of temperature for NV and WP ashes with different concentrations of NaOH. Addition of NaOH as a fluxing agent decreased the viscosity values for both ashes at constant temperature. As presented in

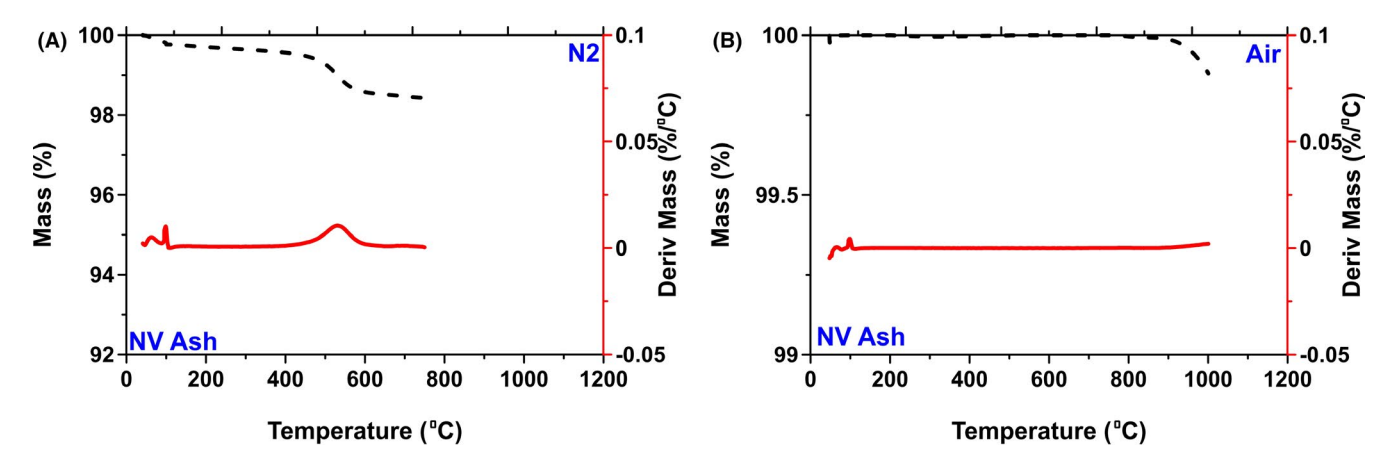


FIGURE 5 2-atmosphere thermogravimetric analysis results of raw NV ash: (A) first step in nitrogen atmosphere, and (B) second step in air; derivative of mass is defined as the absolute value of change in the mass over the change in temperature

Equations 3-6, slag viscosity is highly dependent on slag composition. Additionally, the fluxing agent influenced the slag viscosity values by (a) promoting formation of higher liquid phase content, and (b) changing the composition of slag toward compositions with lower viscosity by increasing the Na⁺ molar fraction.

NV ash (Figure 4A) possessed higher viscosity values compared with WP (Figure 4B). This can be explained using Equation 5 where the slag composition of NV had a higher Si⁴⁺ molar fraction compared to WP, leading to higher viscosity values. Additionally, the mole fraction of Ca²⁺ was relatively negligible for NV compared with WP so that Ca²⁺, which also has a fluxing role, ^{12,23,24} decreased the WP slag viscosity and consequently the solid-liquid suspension viscosity.

3.2 | Gas formation during sintering

3.2.1 Determination of free (unburned) carbon and chemical compounds in raw materials

Heating ash in an oxidizing atmosphere (here, air) leads to decomposition reactions overlapping with carbon oxidation, which makes the determination of the unburned carbon content complex. 29,57 Accordingly, a heating cycle is generally added in an inert atmosphere (here, nitrogen) before the oxidizing atmosphere to prevent carbon oxidation while promoting decomposition reactions. In this study, a two atmosphere TGA (2A-TGA) procedure 57,58 was followed to measure the unburned carbon content. Figures 5 and 6 show the 2A-TGA curves for raw NV and WP ashes, respectively. The unburned carbon content mass fraction for the NV ash was 0.12%, and for the WP ash 0.19%.

Table 3 shows the QXRD results for the raw NV and WP ashes. A higher content of quartz was observed in the NV ash compared with the WP ash, which was consistent with XRF results. 5,12 A higher calcite content was observed for WP obtained by QXRD (see Table 3), which was reflected in the higher CaO content obtained by XRF. In addition, hematite (Fe₂O₃) and anhydrite (CaSO₄) as two possible phases that can contribute to gas release at the sintering temperature were found to be higher for the WP ash compared with the NV ash.

3.3 | Phase development through geopolymerization

Table 4 shows the crystalline phases of geopolymerized NV pellets after 24 hours of curing at 40°C and 30% RH.

The quartz content started to decrease considerably in 16% NaOH addition. The anorthite content decreased and amorphous phase increased with increasing NaOH concentration. Considering the low CaO content (3.51%) of NV bottom ash, a geopolymerization reaction similar to that of class F fly ash⁵⁹ can be considered for NV bottom ash during curing so that the amorphous phase contains N-A-S-H gel.⁶⁰ N-A-S-H gel is formed through breaking Si-O-Si and Si-O-Al (ie, from aluminosilicate sources) bonds into silica and alumina monomers by reacting with OH; further interaction of monomers leads to the formation of dimers, trimers, and/or polymers.⁵⁵

Table 5 shows the crystalline phases and their quantities for WP geopolymerized pellets. With increasing NaOH percentage, the content of the Ca-bearing phases (such as anorthite, calcite, and gehlenite) decreased while the amorphous phase content increased. WP had a high content of CaO (22.5%) and accordingly, it can be considered as a class C fly ash for its geopolymerization reaction with NaOH. In this regard, the alkali cation (Na⁺) acts as a catalyzer via ionic exchange with Ca²⁺ ions. The main product of this reaction is calcium alumina silicate hydrate (C-A-S-H) gel. With reaction progress, small amounts of alkalis can be taken up into the gel structure due to any charge imbalance.⁵⁵ It should be noted that increasing environmental pH (via higher NaOH concentration) favors the formation of C-A-S-H gel, which is probably reflected in the higher amorphous content.61

3.4 | Evaluation of sintering mechanism of geopolymerized pellets using TGA

TGA was performed on the geopolymerized pellets to simulate the sintering process and indirectly identify any possible reactions/decompositions that can lead to the formation of pores in the LWA. Figure 7(A1)-(A4) show the TGA and differential thermogravimetry curves (DTG) for NV ashes prepared with 0%, 4%, 10%, and 16% NaOH concentrations. During the heating ramp, several mass reductions were measured that were associated with DTG peaks. Peak H (40°C to 100°C) was attributed to the release of free water. 62 The increasing trend in peak H by increasing NaOH concentration was mainly associated with the deliquescence effect, ^{63,64} by which the addition of NaOH increased the equilibrium RH in the ash. The second observed peak, that is, G near 100°C to 150°C, was mainly attributed to the release of water from the gypsum structure. 62 The decomposition in the range of 400°C to 550°C (peak C) could be attributed to the decomposition of the amorphous phase in NV ash, most likely C-S-H⁶⁵; the intensity of peak C decreased as NaOH concentration increased in the system preferably implying formations of other amorphous phases (ie, peaks Am₁ and Am₂) in the system. ⁶² Peak

2-atmosphere thermogravimetric analysis results of raw WP ash: (A) first step in nitrogen atmosphere, and (B) second step in air; derivative of mass is defined as the absolute value of change in the mass over the change in temperature

Phases name	Phase formula	Raw NV	Raw WP
Quartz	SiO_2	$18.2 \pm {}^{a}1.7$	8.1 ± 0.3
Katoite	$Ca_3Al_2(SiO_4)_{(3-x)}(OH)_{4x}$ (x = 1.5-3)	0.1 ± 0.1	0.3 ± 0.2
Anhydrite	CaSO ₄	0.4 ± 0.3	1.9 ± 0.2
Merwinite	$Ca_3Mg(SiO_4)_2$	0.0 ± 0	1.2 ± 1.3
Mullite	$3Al_2O_3.2SiO_2$	10.6 ± 2.4	0.9 ± 0.2
Hematite	Fe_2O_3	0.4 ± 0.3	1.0 ± 0.7
Anorthite	$CaAl_2Si_2O_8$	11.2 ± 0.5	8.4 ± 0.8
Brucite	$Mg(OH)_2$	0.1 ± 0.1	0.4 ± 0.2
Portlandite	Ca(OH) ₂	0.0 ± 0.1	0.2 ± 0
Augite	(Ca,Na)(Mg,Fe,Al,Ti) (Si,Al) ₂ O ₆	0.8 ± 0.1	9.4 ± 0.2
Calcite	CaCO ₃	0.9 ± 0.2	4.6 ± 0.7
Gypsum	CaSO ₄ .2H ₂ O	0.4 ± 0.3	0.5 ± 0.4
Anatase	${ m TiO_2}$	1.2 ± 0.1	_
Dolomite	CaMg(CO ₃) ₂	_	0.6 ± 0.2
Gehlenite	Ca ₂ Al[AlSiO ₇]	_	9.8 ± 0.6
Amorphous phase	_	55.6 ± 3	52.9 ± 1.2

Temperature (°C)

TABLE 3 Crystalline phase determination of raw ashes, in mass percent

Temperature (°C)

Am₁ which developed in the higher NaOH samples, could be related to the release of water from amorphous N-A-S-H gel developed through geopolymerization, ⁶⁶ while peak Am₂ was most likely related to the release of water from the amorphous structure of C-A-(N)-S-H type gel. 66,67 The intensity of peak Am2 increased as NaOH increased, which implied that an increasing pH environment favors the formation of C-A-(N)-S-H gel.⁵⁵ No significant decomposition (reaction) was observed after 900°C for the NV samples. The gas release from 1100°C to 1160°C could be considered to contribute to pore formation in the LWA. For NV samples, the mass reductions from 1100°C to 1160°C for NV-0%, NV-4%, NV-10%, and NV-16% were found to be equal to 0.080%, 0.218%, 0.300%, and 0.115%, respectively.

Figure 7B1-B4 show the TGA curves for WP ashes prepared with 0%, 4%, 10%, and 16% NaOH concentrations. Similar to NV ash, the peak H in the WP TGA curves is related to the release of free water, where the height of the peak increased as the NaOH concentration increased mainly due to the deliquescence phenomenon. Peak G was attributed to the release of water from the gypsum structure. Peak C (~350°C to 450°C) was related to the release of water from amorphous C-S-H gel. The decreasing trend of peak C with increasing NaOH concentration implied the transformation of C-S-H

 $^{^{\}mathrm{a}}$ The number after \pm shows one standard deviation of three replicates.

TABLE 4 Crystalline phase of NV geopolymerized pellets, in mass percent

			,		
Crystalline phases	Chemical formula	Raw NV	NV- 4%	NV- 10%	NV- 16%
Quartz	SiO_2	$18.2 \pm {}^{a}1.7$	17.7	17.4	13.7
Anhydrite	CaSO ₄	0.4 ± 0.3	0.3	0.1	0
Merwinite	$Ca_3Mg(SiO4)_2$	0.0 ± 0	0.4	2	3.1
Mullite	$3Al_2O_3.2SiO_2$	10.6 ± 2.4	12.2	8.5	8.0
Hematite	Fe_2O_3	0.4 ± 0.3	0.2	0.7	0.4
Anorthite	CaAl ₂ Si ₂ O ₈	11.2 ± 0.5	8.2	5	6.5
Brucite	$Mg(OH)_2$	0.1 ± 0.1	0.5	0.5	0.6
Portlandite	Ca(OH) ₂	0.0 ± 0.1	0	0.1	0.0
Augite	(Ca,Na)(Mg,Fe,Al,Ti) (Si,Al) ₂ O ₆	0.8 ± 0.1	1.2	1.2	0.7
Calcite	CaCO ₃	0.9 ± 0.2	0.4	0	0
Gypsum	CaSO ₄ .2H ₂ O	0.4 ± 0.3	0.4	0	0.43

 1.2 ± 0.1

 55.6 ± 3

1.2

57.2

2.0

62.5

17

64.8

TiO₂

Anatase

Amorphous

TABLE 5 Crystalline phase of WP geopolymerized pellets, in mass percent

Crystalline phases	Chemical formula	Raw WP	WP- 4%	WP- 10%	WP- 16%
Quartz	SiO_2	8.1 ± 0.3^{a}	8.8	6.1	5.8
Katoite	$Ca_3Al_2(SiO_4)_{(3-x)}(OH)_{4x}$ (x = 1.5-3)	0.3 ± 0.2	0.1	0.3	0.3
Anhydrite	CaSO ₄	1.9 ± 0.2	1.4	1.5	1.4
Merwinite	$Ca_3Mg(SiO_4)_2$	1.2 ± 1.3	0.8	1.3	1.9
Mullite	$3Al_2O_3.2SiO_2$	0.9 ± 0.2	0.9	0.9	0.4
Hematite	Fe_2O_3	1.0 ± 0.7	0.5	0.4	0.2
Anorthite	$CaAl_2Si_2O_8$	8.4 ± 0.8	5.5	3.2	3.4
Brucite	$Mg(OH)_2$	0.4 ± 0.2	0.6	0.6	0.8
Portlandite	Ca(OH) ₂	0.2 ± 0	0	0.1	0
Augite	(Ca,Na)(Mg,Fe,Al,Ti) (Si,Al) ₂ O ₆	9.4 ± 0.2	7.6	6.6	5.9
Calcite	CaCO ₃	4.6 ± 0.7	5.8	3.0	1.7
Gypsum	CaSO ₄ .2H ₂ O	0.5 ± 0.4	0.5	0.8	0.4
Dolomite	CaMg(CO ₃) ₂	0.6 ± 0.2	0	0	0.3
Gehlenite	Ca ₂ Al[AlSiO ₇]	9.8 ± 0.6	8.3	7.3	5.4
Amorphous	_	52.9 ± 1.2	59.4	67.7	72.1

 $^{^{}a}$ The number after \pm shows one standard deviation of three replicates.

towards formation of C-A-(N)-S-H gel (ie, peak Am_2) for the WP samples. Additional peaks of C', CH, and θ were observed that were most likely related to, respectively: (a) the presence of another form of C-S-H gel with different Si/Ca ratio than that of peak C leading to a different thermal decomposition range, 62 (b) the decomposition of portlandite in geopolymerized pellets at ~450°C, 62 and (c) calcite (CaCO₃) decomposition and emission of CO₂ gas at ~620°C to 750°C. 62 Peak C' disappeared as the NaOH concentration increased to form

C-A-(N)-S-H gel (peak Am₂). Peak –C also decreased as the NaOH concentration increased (the trend was also consistent with that of measured by QXRD, see Table 4), where calcite as a Ca-bearing phase was consumed to form C-A-(N)-S-H gel (peak Am₂). Therefore, the intensity of the Am₂ peak increased as the NaOH concentration increased, which was compatible with the QXRD result (see Table 4) that there was an increase in amorphous phase content as the NaOH concentration increased. In contrast with the NV geopolymerized

^aThe number after ± shows one standard deviation of three replicates.

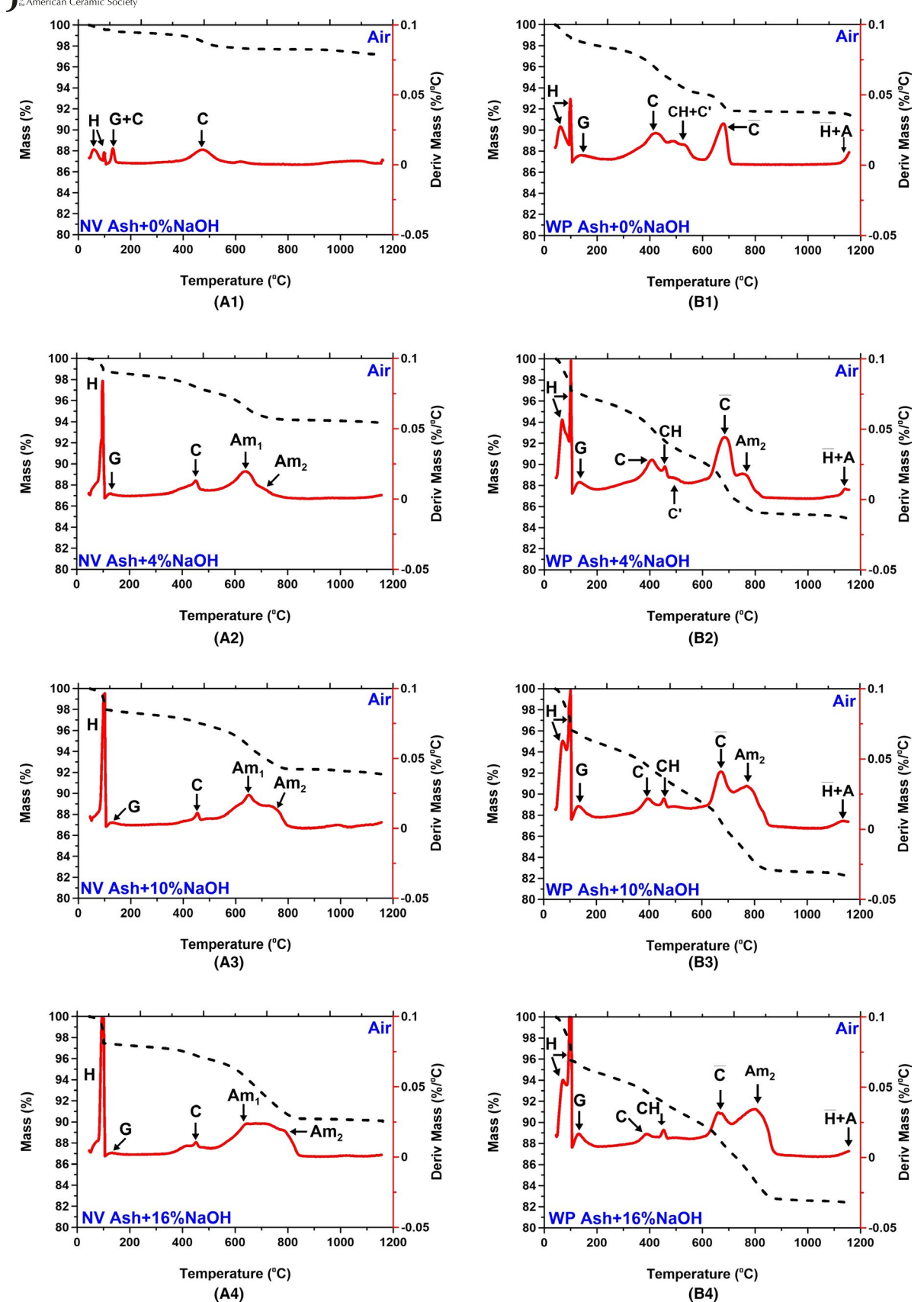


FIGURE 7 Thermogravimetric analysis/differential thermogravimetry curves curves for NV and WP geopolymerized pellets with varying concentrations of NaOH measured in air (H: H₂O, G: Gypsum, C: C-S-H, C': (C-S-H)', Am₁:N-A-S-H, -C: CaCO3, Am₂: C-(N)-A-S-H, -H: Hematite, A: Anhydrate; derivative of mass is defined as the absolute value of change in the mass over the change in temperature

pellets, a decomposition reaction could be observed in the WP pellets near 1160°C as demonstrated by peak + -CA. Peak + -HA is most likely associated with the release of gaseous phases from hematite and anhydrite. ^{34,68} The mass reductions recorded between 1100°C and 1160°C for WP-0%, WP-4%, WP-10%, and WP-16% were equal to 0.55%, 0.48%, 0.45%, and 0.33%, respectively.

It was hypothesized that due to the rapid sintering of LWA for 4 minutes, dihydroxylation (ie, the release of water) of amorphous phases available in the geopolymerized NV and WP samples may shift towards higher temperatures and accordingly can contribute to the formation of pores near sintering temperatures (~1160°C). To test this hypothesis, a heating ramp of 100°C/min (equal to the safe maximum capacity of the TGA device) was used to mimic the rapid sintering of LWA in TGA for NV-10% and WP-10%. The results are plotted in Figure 8A and B with dashed and solid green lines for TGA and DTG curves, respectively. A slight temperature shift of peaks was observed by \approx –H30°C⁶²; however, no contribution from dehydroxylation (gaseous H₂O release) of amorphous phases was observed near 1160°C to contribute to pore formation during sintering.

3.5 | Evaluation of pore structure using X-CT

To observe the effect of sintering on LWA pore formation, X-CT was carried out, before and after sintering, for the NV-10% and WP-10% samples. The X-CT results for the geopolymerized NV-10% and WP-10% samples (ie, before sintering) are shown in Figures 9 and 10, respectively. Plane A A and B B were selected to represent the middle cross-section of LWA in two perpendicular directions. Light color defines regions with denser structure (ie, solid phase) while darker color demonstrates regions with lesser density (ie, pores). 2D slices of samples in both geopolymerized samples (Figures 9 and 10) only contained coarse (ie, random shape) pores, resulting from the coarse granular structure of bottom ash during the sample preparation. Figures 11 and 12 show the X-CT results of sintered samples for NV and WP LWA, respectively, made with 4%, 10%, and 16% NaOH concentration. Comparing 2D slices before and after sintering for a sample made using 10% NaOH, the porosity of LWA had increased by the end of the sintering process. The porosities of non-sintered NV-10% and WP-10%, which was measured using image analysis of XCT slices as the total volume of pores divided by the total volume of LWA and reported as percentage (detailed procedure of porosity calculations can be found in Ref. [5]), were 36.4% and 36.3%, respectively. After sintering, NV-10% and WP-10% had porosities equal to 44% and 41.6%, respectively, as the formation of large pores could increase the porosity of LWA. Videos demonstrating the porous structure of all LWA made in this study were provided in Table S1 of the Supplemental Materials.

Generally, two zones can be identified on the 2D slices (except for NV-4% and WP-4%, most probably due to the lack of a liquid phase) of LWA, separated by white dashed lines (shown in Figures 11 and 12). The inner part is referred to as "core," while the outer part is referred to as "shell." For both LWA types shown in Figures 11 and 12, the rounded large pores were mainly formed in the shell region of the LWA. In contrast, the core appears to possess interconnected smaller pores that were not specifically created by gas release but rather by the sintering and grain growth mechanism.⁶⁹ A possible explanation for the different morphologies of LWA core and shell could be that the shell acted as an insulating layer, delaying heat transfer to the LWA core and also limiting the diffusion of oxygen to the core. 18,68 This phenomenon can lead to occurrence of a reducing atmosphere in the core of LWA while having a highly oxidizing atmosphere for the shell. 70 In addition, coalescence of the pores (ie, pores jointing together) in the shell⁶⁹ led to the formation of stable pores with a larger volume.

Enlarged images of the A_A 2D slices for NV-10% and WP-10%, LWA core and shell are provided in Figure 13. The shell material around the large pores is denser than the core material in both LWA. It is speculated that the shell material not only provides the structural integrity for the LWA, but it may also help to strengthen the LWA.

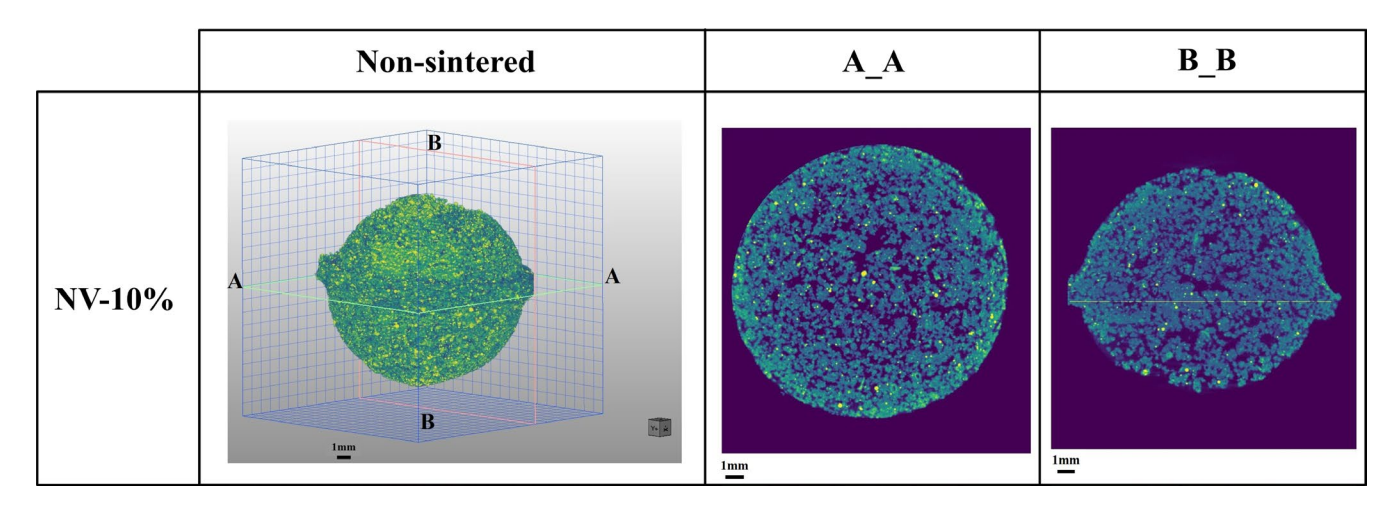
4 | DISCUSSION

This section scrutinizes the production of LWA with respect to the three required conditions (ie, sufficient liquid phase formation, appropriate viscosity for solid-liquid phase, and adequate gas release) and correlates each of them with observations made from the XCT images. In addition, a diagram to predict successful LWA production is discussed.

4.1 | Formation of liquid phase during sintering

Formation of a sufficient amount of liquid phase on the LWA surface to entrap the emitted gaseous phases is a critical condition that needs to be achieved during sintering for successful LWA pore formation. Figure 14 shows the amount of the liquid phase at 1160°C for the LWA investigated. An increase in the NaOH concentration resulted in a higher liquid phase content for both LWA made using NV and WP ashes. NaOH has a lower melting temperature compared with

Thermogravimetric analysis (TGA)/ differential thermogravimetry curves (DTG) curves for NV and WP geopolymerized pellets with 10% NaOH; the red lines are associated with a heating ramp of 20°C/minute while green lines indicate the TGA and DTG curves associated with a heating ramp of 100°C/min



Three-dimensional reconstruction and two-dimensional slices of NV-10% pellet after geopolymerization and before sintering; Plane A_A and B_B were selected to represent the middle cross-section of lightweight aggregate

the multi-component ash system; therefore, it provides a medium for easier ion diffusion and grain growth resulting in a lower melting temperature of the ash and NaOH blend. For NV-0%, as shown in Figure 14, the liquid phase content was <3% while addition of 4% NaOH increased the liquid phase content for NV-4% to 47.2%. Correlating this observation with 3D X-CT reconstruction and A_A and B_B 2D slices of NV-4% provided in Figure 11, no large rounded pore was observed for NV-4% LWA. This finding implies that although some gas release has occurred during sintering, the low liquid phase content could not entrap the emitted gaseous phases. When the liquid phase was raised to 50% in NV-10% and more prominently in NV-16%, even a small amount of gas release could be entrapped by the liquid phase and larger pores formed (Figure 11, see A_A and B_B 2D slices of NV-10% and NV-16%).

Temperature (°C)

Similar to the case of the NV ash, the addition of 4% NaOH increased the liquid phase content for WP-4% LWA to 58.3% while for WP-0% this value was only 10.3%. As observed in the 2D slices of the WP-4% LWA in Figure 12, the amount of liquid phase was sufficient to successfully entrap the released gas during sintering near 1160°C. Also similar to the NV LWA, an increase in NaOH concentration increased the quantity of the liquid phase at 1160°C. Correlating the visualized 2D slices of WP LWA (see Figure 12) with the liquid phase content, it can be inferred that higher content of liquid phase triggered the higher amount of gaseous phase entrapment, and consequently larger pores were formed. However, it should be noted that an excess amount of liquid phase may create deformation in the sintered LWA due to unnecessary reduction in the liquid-solid viscosity (as will be discussed later) and the desired sphericity may not be

Temperature (°C)

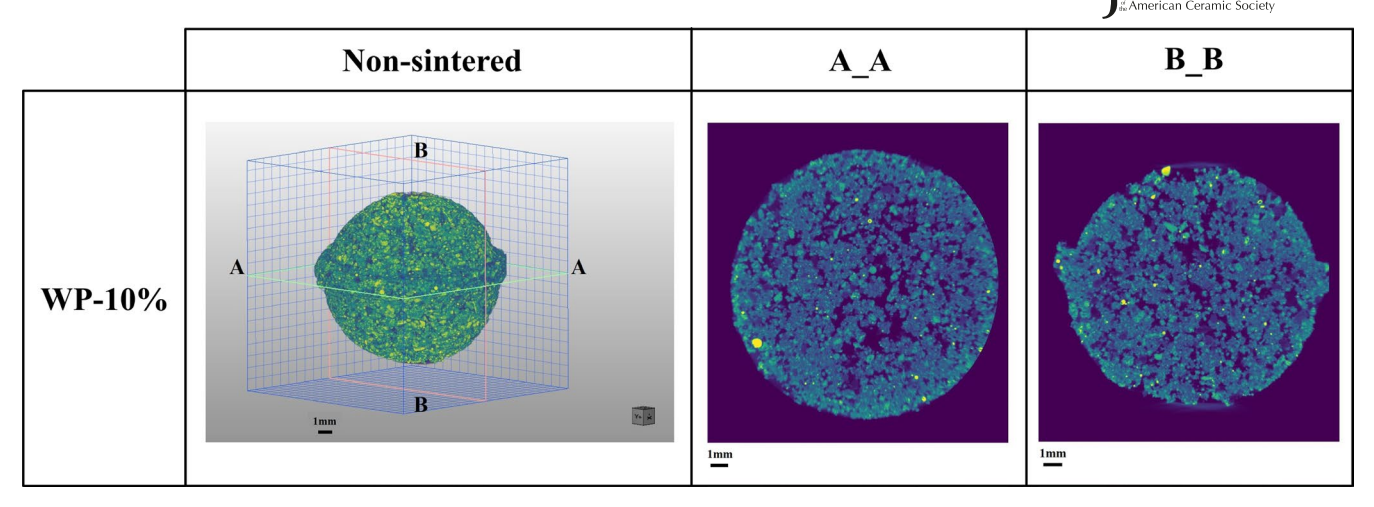


FIGURE 10 Three-dimensional reconstruction and two-dimensional slices of WP-10% pellet after geopolymerization and before sintering; Plane A_A and B_B were selected to represent the middle cross section of lightweight aggregate

achieved during the sintering process, as observed in sample WP-16% in Figure 12. It appears that a minimum amount of 50% liquid content (shown by green dashed line in Figure 14) is necessary during sintering bottom ashes to provide sufficient particle binding along with bloating (look at 2D slices in Figures 11 and 12, in which the LWA with more that 50% liquid phase demonstrated formation of round large pores in the shell).

4.2 | Viscosity of liquid-solid phase during sintering

Viscosity plays two simultaneous roles in successful LWA production. First, a high viscosity prevents excessive deformation of the LWA pellet during sintering so that the final product retains a round shape. Second, the viscosity of the liquid phase affects the LWA pore size distribution. Correlating the 3D reconstructions (Figure 11) and viscosity values for NV LWA (Figure 4A), it can be inferred that the viscosity of the NV LWA was high enough to limit the deformation of LWA so as to preserve a spherical shape. Although the WP LWA had lower viscosity values (Figure 4B) compared with the NV LWA, the same observation was made for WP-4% and WP-10%. The only WP LWA that had excessive deformation under gravitational force was WP-16%, which had a viscosity of 25.7 Pa·s at 1160°C and a final elliptical shape. It appears a lower limit for liquid-solid viscosity is near that of WP-10%, which was 85 Pa·s, in order to retain the LWA spherical shape during sintering.¹²

The second role of the viscosity in controlling the pore size distribution can be observed in the A_A and B_B 2D projections of the NV and WP LWA in Figures 11 and 12, respectively, where larger pores were formed in the WP LWA compared to the NV LWA. Since NV LWA had a higher

viscosity compared with WP LWA, lower viscosity seemingly led to easier expansion of gas inside the liquid phase, resulting in the formation of larger pores. This observation can also be related to amount of gaseous release²² close to the sintering temperature, which will be discussed in the following section. It is worth mentioning that another important factor that can affect the pore size in the LWA is the pressure difference inside the pore and liquid phase which is determined by the Laplace pressure. Based on the Laplace equation this pressure difference is dependent on the pore diameter and the surface tension of the interface between the gas inside the pore and the liquid phase.⁷¹ It should be noted that the surface tension is also dependent on the viscosity of the liquid phase.⁷²

4.3 | Formation of gaseous phase during sintering

As was observed in Figure 7, the TGA/DTG results showed a more pronounced peak at 1160°C for the WP LWA compared with the NV LWA. The mass reduction from 1100°C to 1160°C is believed to be associated with hematite and anhydrite compounds, the presence of which was confirmed by QXRD, to release O₂ and SO₂ gases, respectively. ^{34,70} Both anhydrite and hematite were detected in raw ashes as well as in geopolymerized pellets (see Tables 2-4). Moreover the anhydrite content for the NV geopolymerized pellets was found to be smaller than in the WP pellets. This observation supports the fact that WP LWA have a higher potential for gas liberation at 1160°C, which can be another possible explanation for the formation of bigger pores in WP LWA compared with NV LWA. 22,73 The reactions that can lead to gas liberation from the transition of hematite from Fe³⁺ to Fe²⁺ can happen through Equations 1 and 2, while the



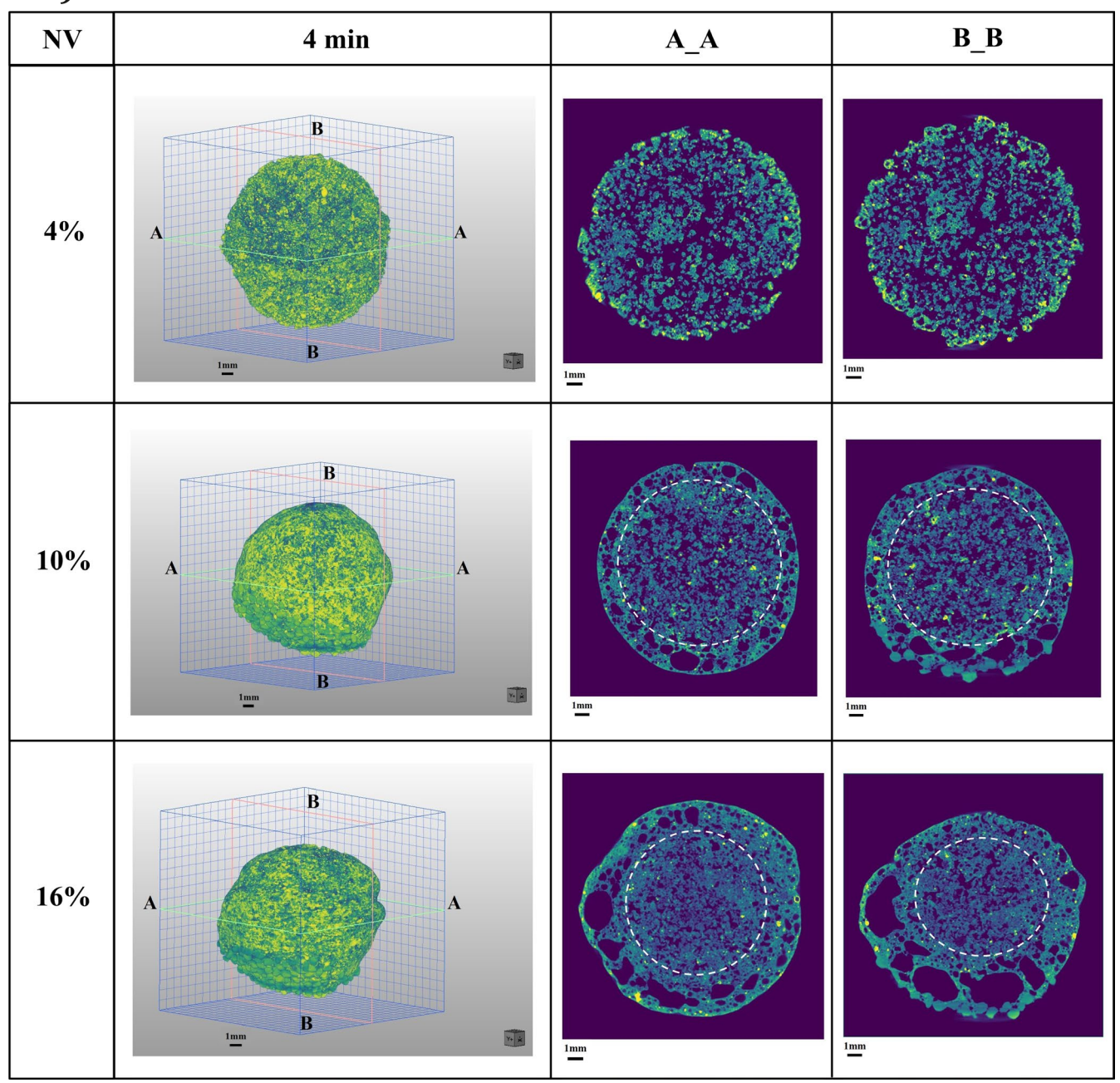


FIGURE 11 Three-dimensional reconstruction and two-dimensional slices of NV sintered lightweight aggregate (LWA) for 4 min; Plane A_A and B_B were selected to represent the middle cross section of LWA

reaction for anhydrite decomposition can be expressed as follows:

$$CaSO_{4}(s) \rightarrow CaO(s) + SO_{2}(g) + \frac{1}{2}O_{2}(g)$$
 (8)

As was observed in the DTG curves for WP geopolymerized pellets (Figure 7A1-A4), the peak at 1160°C seems incomplete, that is, the temperature was not high enough to enable complete decomposition. This may be attributed to the fact that a complete decomposition of CaSO₄ occurs at temperatures above 1200°C.^{74,75} A possible explanation for the reduction of hematite into wuestite

(FeO) that could occur at a temperature range between 1100°C and 1160°C is the formation of liquid phase on the LWA surface that could hinder oxygen diffusion and create a reducing atmosphere in the LWA core, thus leading to hematite reduction.^{7,76}

In this study, the unburned carbon content for NV and WP ashes was small (0.12% and 0.19%, respectively), and complete oxidation of carbon in the form of CO₂ and CO release would happen at temperatures below 1000°C²⁹ (see Figures 5 and 6), which had some overlap with the temperature at which the liquid phase started to form (see Figure 3). This indicates that there could have been some contribution from

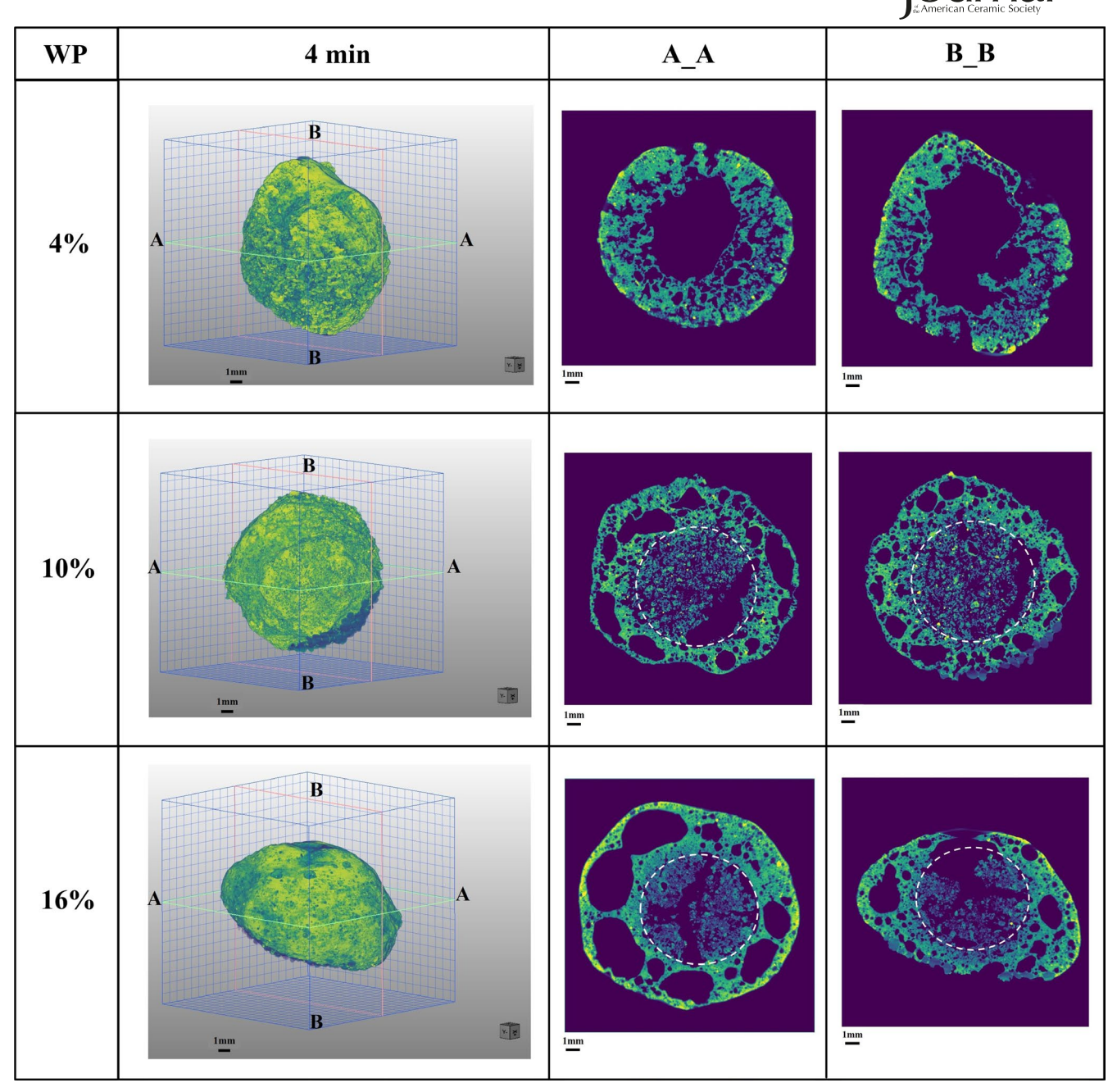


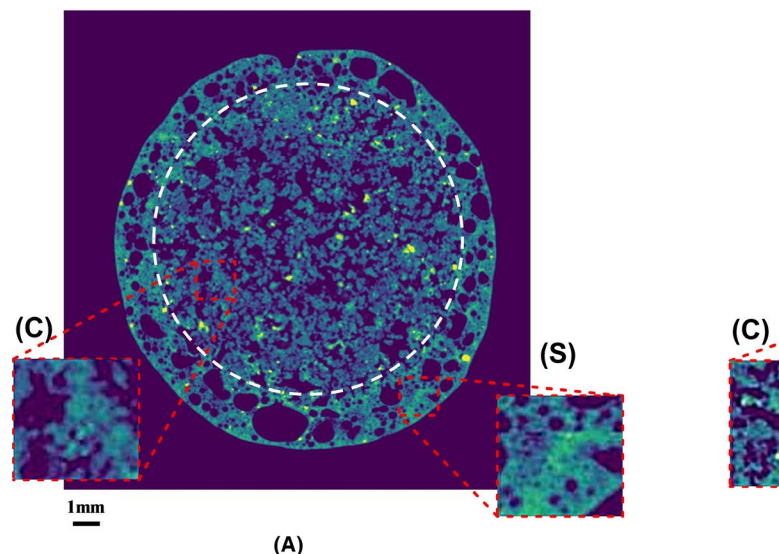
FIGURE 12 Three-dimensional reconstruction and two-dimensional slices of WP sintered lightweight aggregate (LWA) for 4 min; Plane A_A and B_B were selected to represent the middle cross section of LWA

the unburnt carbon to reduce the hematite and result in the release of ${\rm O_2}.^{68,76,77}$

4.4 | Required sintering conditions for successful production of spherical LWA

Figure 15 presents a holistic view of each LWA to provide the required conditions (liquid phase quantity, viscosity value, and emitted gas amount) during sintering for successful production of spherical LWA. It should be noted that NV-0% and WP-0% are not shown in the

figure, since due to the lack of liquid phase their viscosity was not calculable (see Viscosity Calculation). It is proposed that a minimum value of 50% liquid content (shown by red dashed line in Figure 15) and a minimum viscosity value of 100 Pa·s (shown by blue dashed line in Figure 15) are required for successful LWA production. For NV LWA, NV-0% and NV-4%, which had an inadequate amount of liquid phase (ie, <50%), formation of rounded large pores was not observed in the X-CT images. The same observation was made for WP-0%, which also had an insufficient amount of liquid phase. On the other hand, for NV-10%, NV-16%, WP-4%, and



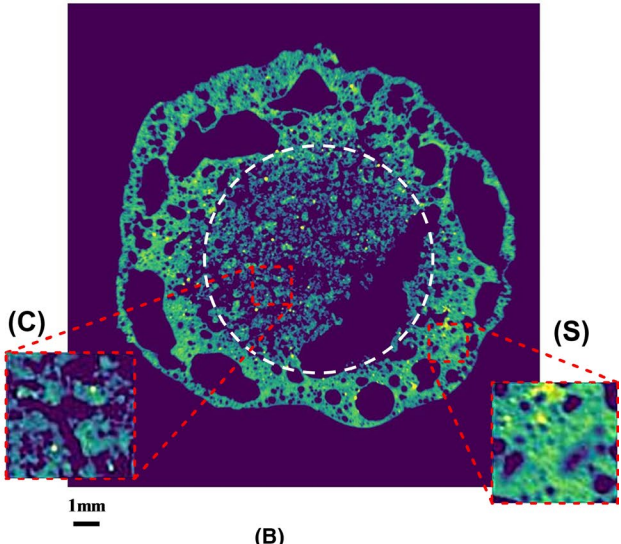


FIGURE 13 A_A 2D slices of (a) NV-10% and (b) WP-10%; enlarged sections of the core and shell are indicated by (C) and (S), respectively

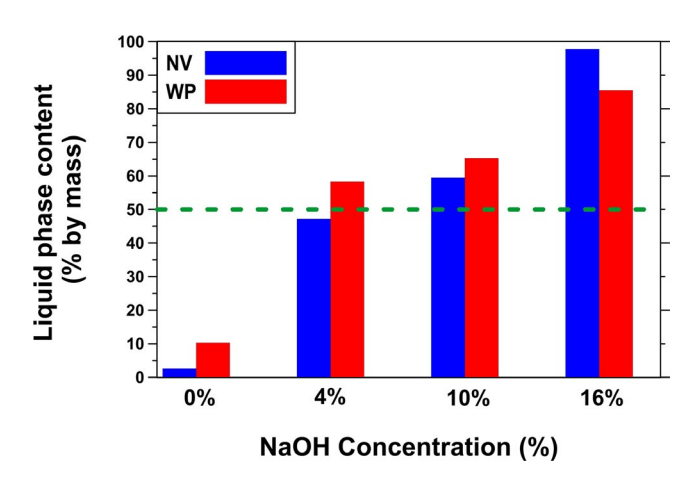


FIGURE 14 Quantity of the liquid phase for NV and WP LWA at 1160°C obtained using thermodynamic simulations (green dashed line shows the 50% limit)

WP-10%, a sufficient amount of liquid phase (50% or more) accompanied with proper viscosity values (more than 100 Pa·s), led to LWA production with the desired pore structure and particle sphericity. However, for WP-16%, the viscosity value was about 26 Pa·s, which led to the deformation of the LWA under gravitational force and an undesired elliptical shape (see Figure 12). Based on Billen et al's melt ceramic model, ¹² an upper limit value of 10⁶ Pa·s was proposed (shown by blue dashed line in Figure 15) to ensure a viscosity for the liquid phase to be able to entrap the gaseous phase and let the pellets expand during sintering. The value of 10⁶ Pa·s is between the viscosity values of NV-4% and NV-10%, and implied that a NaOH concentration between 4% and 10% will probably result in the entrapment of pores in the

LWA. Further research is needed to accurately determine this upper viscosity limit. Figure 15 could be used to design a successful LWA with respect to the three required conditions: sufficient amount of liquid phase, appropriate viscosity for solid-liquid suspension, and sufficient amount of gas release. If an LWA has the key three characteristics such that it falls in the working zone proposed in Figure 15, it can be expected to be a desirable LWA.

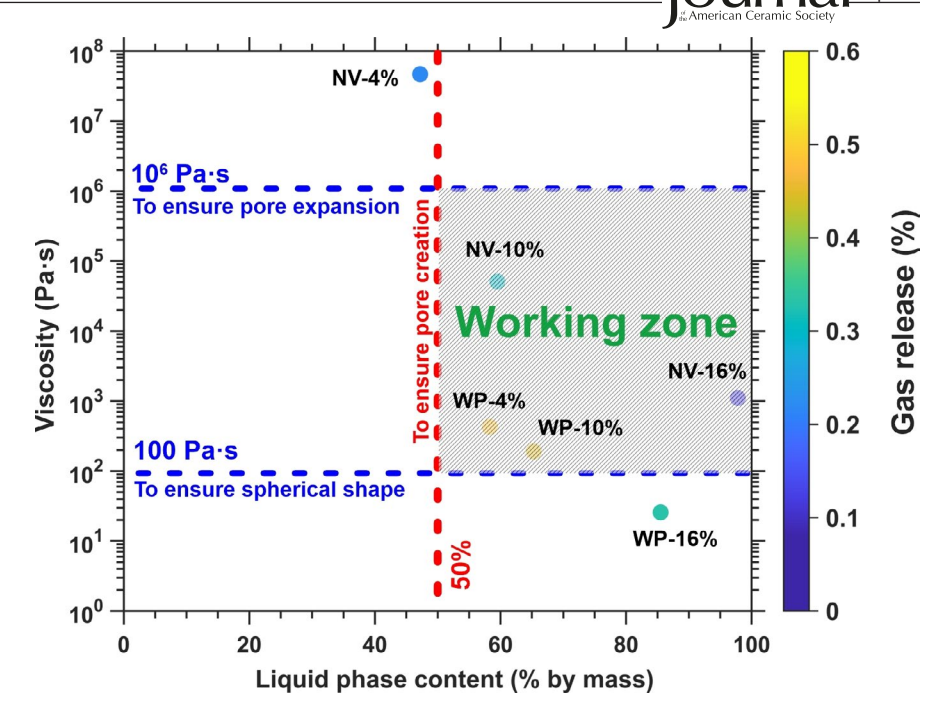
5 | CONCLUSION

This paper investigated the three required conditions that need to be achieved during sintering for successful LWA production from waste coal bottom ash: (a) formation of a sufficient amount of the liquid phase, (b) achievement of an appropriate viscosity for the combined liquid-solid phase, and (c) emission of a sufficient amount of gaseous phase. Two types of coal bottom ash, low-calcium (NV) and high-calcium (WP), were studied to evaluate these three sintering conditions. The following main conclusions can be drawn from this study regarding the three necessary conditions for successful sintering/LWA production:

1. The presence of at least 50% (by mass) liquid phase enables successful gas entrapment and LWA pore formation. It was observed that for NV-4%, in which the liquid phase content was <50%, no gas-filled rounded pores could be seen achieved in the LWA pore structure. However, all LWA with more than 50% liquid phase during sintering possessed round gas-filled pores in their structure (mainly in the outer shell part of the LWA structure).</p>

Iournal 19

FIGURE 15 Shaded area shows the proposed representation of the conditions (ie, liquid phase quantity, viscosity, and gas release) required for successful lightweight aggregate production



- 2. The viscosity of the liquid-solid suspension was found to influence LWA pore formation and control LWA deformation during sintering. A minimum viscosity of 100 Pa·s was found to be necessary to retain the spherical shape of the LWA pellets during sintering. Above this minimum value, the WP LWA, which had smaller viscosity values compared with the NV LWA, possessed larger gas-filled pores. Lower viscosity values not only allow easier movement of pores to coalesce, but also easier expansion of entrapped gases in the liquid phase medium. An upper limit of 10⁶ Pa·s was proposed for the liquid-solid phase in order to still be able to entrap emitted gases.
- 3. It was found that the emission of gaseous phases near the sintering temperature is necessary to create the desired LWA pore structure, given that the desired liquid phase content and viscosity values listed in (i) and (ii) are also achieved during sintering. All LWA demonstrated gas liberation near the sintering temperature where WP LWA showed a slightly higher amount of gaseous phase formation compared with NV LWA. The emitted gaseous phase was found to be most probably due to the reduction of hematite and the decomposition of anhydrite. Gas emission from other sources was at temperatures not near enough to the sintering temperature to be helpful in forming pores.

A diagram incorporating the three required conditions for successful production of LWA, ie, formation of enough liquid phase, appropriate solid-liquid viscosity, and enough gas emission, was developed, and a working zone defined in the diagram. The working zone was constrained by a liquid phase of more than 50%, and a viscosity upper limit of 10^6 Pa·s and a lower limit of 100 Pa·s. The diagram and the working zone predict whether the production of a LWA will be successful or not.

From a practical point of view and environmental perspective, a smaller NaOH concentration not only reduces the cost associated with LWA production, but also decreases the greenhouse gas emissions accrued during NaOH production. For successful LWA production from NV and WP ashes, a NaOH concentration by mass between 4% and 10% was found to be an appropriate concentration range of this fluxing agent to achieve the desired three sintering conditions for successful LWA production at 1160°C.

Future work is needed to investigate the bubble nucleation and growth mechanism in the LWA liquid phase and the kinetics that impose different atmospheres in the shell and in the core of the LWA. Future work may also involve evaluating the mechanical strength of the LWA made using bottom ash and its correlation with parameters such as chemical composition, crystalline structure, liquid phase quantity, and porosity. Preliminary results indicate that SPoRA has a comparable compressive strength with commercially available LWA; therefore, it is expected that SPoRA can be successfully used to produce lightweight concrete. If the LWA is used to produce lightweight concrete, the bonding performance of LWA with cement paste and characteristics of the Interfacial Transition Zone (ITZ) in the concrete need to be investigated to fully understand the LWA-cement paste physical and mechanical interaction.

One of the major concerns in recycling or beneficial use of bottom ash is related to leaching of heavy metals from this material. The production of LWA using a sintering method from different base materials (such as municipal solid waste incinerator ash, sewage sludge ash, fly ash, and bottom ash) that contain heavy metals, have been shown to be a potentially successful approach to decrease the leachability of heavy metals from these materials. This

is because of the fact that sintering of materials at high temperature (ie, greater than 1100°C) enables liquid phase formation and then crystalline phase formation upon cooling. This can potentially lead to solidification of heavy metals by being bonded in the crystal structure. The work may also involve investigating the potential advantage of producing LWA from bottom ash using a sintering method to reduce the leachability of heavy metals from this material. Finally, the use of bottom ash to produce LWA can help to minimize the use of natural resources (eg clay, shale, and slate) to produce synthetic LWA for construction needs.

ACKNOWLEDGMENT

The work presented here was supported in part by the National Science Foundation (NSF CMMI – 1550723 and PFI– TT 1918838) and was performed at Drexel University in the Advanced and Sustainable Infrastructure Materials (ASIM) Lab. Any opinions, findings, and conclusions or recommendations expressed in this material are those of the authors and do not necessarily reflect the views of the National Science Foundation.

ORCID

Mohammad Balapour https://orcid.org/0000-0002-0133-2440

REFERENCES

- 1. Association ACA. ACAA 2018 CCP Survey Results; 2018.
- Giusti L. A review of waste management practices and their impact on human health. Waste Manag. 2009;29:2227–39.
- O'Hare KJ, Pizzulli G, Torelli M, Balapour M, Farnam Y, Grace Hsuan Y, et al. Life cycle assessment of lightweight aggregates from coal ashes: a cradle-to-gate analysis BT. In: Kovler K, Zhutovsky S, Spatari S, Jensen OM, editors. Concrete durability and service life planning. Cham: Springer International Publishing; 2020, p. 47–51.
- EPA. 40 CFR Parts 257 and 261: hazardous and solid waste management system: disposal of coal combustion residues from electric utilities. Fed Regist. 2015;(80):21302–501.
- Balapour M, Zhao W, Garboczi EJ, Oo NY, Spatari S, Hsuan YG, et al. Potential use of lightweight aggregate (LWA) produced from bottom coal ash for internal curing of concrete systems. Cem Concr Compos. 2020;105:103428.
- Aineto M, Acosta A, Rincón JM, Romero M. Production of lightweight aggregates from coal gasification fly ash and slag. Lexington, KY, USA: World Coal Ash; 2005; p. 11–5.
- Dondi M, Cappelletti P, D'Amore M, de Gennaro R, Graziano SF, Langella A, et al. Lightweight aggregates from waste materials: reappraisal of expansion behavior and prediction schemes for bloating. Constr Build Mater. 2016;127:394

 –409.
- Korat L, Ducman V, Legat A, Mirtič B. Characterisation of the pore-forming process in lightweight aggregate based on silica sludge by means of X-ray micro-tomography (micro-CT) and mercury intrusion porosimetry (MIP). Ceram Int. 2013;39:6997–7005.

- Franus W, Jozefaciuk G, Bandura L, Franus M. Use of spent zeolite sorbents for the preparation of lightweight aggregates differing in microstructure. Minerals. 2017;7:25–39.
- Balapour M, Rao R, Spatari S, Hsuan YG, Farnam Y. Engineering Properties of Fly Ash-Based Lightweight Aggregate. World Coal Ash Conf. (WOCA), St. Louis, MO, May 13–16, 2019.
- 11. Wei Y-L, Lin Y-Y. Role of Fe compounds in light aggregate formation from a reservoir sediment. J Hazard Mater. 2009;171:111–5.
- Billen P, Mazzotti M, Pandelaers L, Ye oo N, Zhao W, Liu Z, et al. Melt ceramics from coal ash: constitutive product design using thermal and flow properties. Resour Conserv Recycl. 2018;132:168–77.
- Johansson L. The use of LECA (Light Expanded Clay Aggregates) for the removal of phosphorus from wastewater. Water Sci Technol. 1997;35:87–93.
- Standard A. Standard specification for lightweight aggregate for internal curing of concrete. West Conshohocken: Annu B ASTM Stand ASTM Int; 2013.
- Boudaghpour S, Hashemi S. A study on light expended clay aggregate (LECA) in a Geotechnical view and its application on greenhouse and greenroof cultivation. Int J Geol. 2008;4:59–63.
- Test CC, Mortar H, Concrete C, Specimens CC, Concrete L, Freezing R, et al. Standard Specification for Lightweight Aggregates for Structural Concrete. 2011;1–4.
- 17. Ostrowska K, Janczukowicz W, Białowiec A, Rodziewicz J. Nitrogen removal in vertical-flow filters filled with lightweight aggregate made of fly ashes and gravel. J Environ Eng. 2013;139:1266–72.
- 18. Ducman V, Korat L, Legat A, Mirtič B. X-ray micro-tomography investigation of the foaming process in the system of waste glass–silica mud–MnO2. Mater Charact. 2013;86:316–21.
- van Dyk JC, Waanders FB, Benson SA, Laumb ML, Hack K. Viscosity predictions of the slag composition of gasified coal, utilizing FactSage equilibrium modelling. Fuel. 2009;88:67–74.
- Torelli M. A thermodynamic modeling approach for environmentally optimized prospective design of spherical porous reactive aggregates, Master Thesis. Drexel University; 2019.
- Romero M, Andrés A, Alonso R, Viguri J, Rincón JM. Sintering behaviour of ceramic bodies from contaminated marine sediments. Ceram Int. 2008;34:1917–24.
- Prousevitch AA, Sahagian DL, Anderson AT. Dynamics of diffusive bubble growth in magmas: isothermal case. J Geophys Res Solid Earth. 1993;98:22283–307.
- Riley CM. Relation of chemical properties to the bloating of clays.
 J Am Ceram Soc. 1951;34:121–8.
- Browning GJ, Bryant GW, Hurst HJ, Lucas JA, Wall TF. An empirical method for the prediction of coal ash slag viscosity. Energy Fuels. 2003;17:731–7.
- 25. Urbain G. Viscosity estimation of slags. Steel Res. 1987;58:111-6.
- Rincón A, Marangoni M, Cetin S, Bernardo E. Recycling of inorganic waste in monolithic and cellular glass-based materials for structural and functional applications. J Chem Technol Biotechnol. 2016;91:1946–61.
- 27. Bernardo E, Cedro R, Florean M, Hreglich S. Reutilization and stabilization of wastes by the production of glass foams. Ceram Int. 2007;33:963–8.
- Appendino P, Ferraris M, Matekovits I, Salvo M. Production of glass-ceramic bodies from the bottom ashes of municipal solid waste incinerators. J Eur Ceram Soc. 2004;24:803–10.

- Paya J, Monzo J, Borrachero MV, Perris E, Amahjour F. Thermogravimetric methods for determining carbon content in fly ashes. Cem Concr Res. 1998;28:675–86.
- 30. Parkinson GS. Iron oxide surfaces. Surf Sci Rep. 2016;4:1-165.
- Wie YM, Lee KG. Optimum bloating-activation zone of artificial lightweight aggregate by dynamic parameters. Materials (Basel). 2019;12:267.
- 32. Wei Y-L, Yang J-C, Ko K-W. Evidence for a new mechanism of Fe 2 O 3 decomposition in lightweight aggregate formation. Environ Chem Lett. 2012;10:41–7.
- 33. Wei Y-L, Cheng S-H, Ou K-T, Kuo P-J, Chung T-H, Xie X-Q. Effect of calcium compounds on lightweight aggregates prepared by firing a mixture of coal fly ash and waste glass. Ceram Int. 2017;43:15573–9.
- Salman OA, Khraishi N. Thermal decomposition of limestone and gypsum by solar energy. Sol Energy. 1988;41:305–8.
- Einstein A. Eine neue bestimmung der moleküldimensionen. Ann Phys. 1906;324:289–306.
- Liu Z, Blanpain B, Guo M. Viscosity of heterogeneous silicate melts: a non-newtonian model. Metall Mater Trans B. 2017;48:3027–37.
- 37. Part WK, Ramli M, Cheah CB. An overview on the influence of various factors on the properties of geopolymer concrete derived from industrial by-products. Constr Build Mater. 2015;77:370–95.
- 38. Bale CW, Bélisle E, Chartrand P, Decterov SA, Eriksson G, Hack K, et al. FactSage thermochemical software and databases—recent developments. Calphad. 2009;33:295–311.
- Bale CW, Chartrand P, Degterov SA, Eriksson G, Hack K, Ben Mahfoud R, et al. FactSage thermochemical software and databases. Calphad. 2002;26:189–228.
- Bale CW, Bélisle E, Chartrand P, Decterov SA, Eriksson G, Gheribi AE, et al. Reprint of: FactSage thermochemical software and databases, 2010–2016. Calphad. 2016;55:1–19.
- 41. Hanxu LI, Yoshihiko N, Zhongbing D, Zhang M. Application of the FactSage to predict the ash melting behavior in reducing conditions. Chinese J Chem Eng. 2006;14:784–9.
- D4326-13 A. Standard Test Method for Major and Minor Elements in Coal and Coke Ash By X-Ray Fluorescence. ASTM Int Stand 2013
- Song W, Sun Y, Wu Y, Zhu Z, Koyama S. Measurement and simulation of flow properties of coal ash slag in coal gasification. AIChE J. 2011;57:801–18.
- 44. Watt JD, Fereday F. The flow properties of slag formed from the ashes of British coals. J Ind Fuel. 1969;42:131–4.
- 45. Kondratiev A, Jak E. Predicting coal ash slag flow characteristics (viscosity model for the Al2O3–CaO–'FeO'–SiO2 system). Fuel. 2001;80:1989–2000.
- Nicholls P, Reid WT. Viscosity of coal-ash slags. J Eng Power; (United States). 1940;62:141–53.
- Krieger IM, Dougherty TJ. A mechanism for non-Newtonian flow in suspensions of rigid spheres. Trans Soc Rheol. 1959;3:137–52.
- 48. Stovall T, De Larrard F, Buil M. Linear packing density model of grain mixtures. Powder Technol. 1986;48:1–12.
- Bullard JW, Pauli AT, Garboczi EJ, Martys NS. A comparison of viscosity–concentration relationships for emulsions. J Colloid Interface Sci. 2009;330:186–93.
- Doebelin N, Kleeberg R. Profex: a graphical user interface for the Rietveld refinement program BGMN. J Appl Crystallogr. 2015;48:1573–80.

- 51. Shields Y, Garboczi E, Weiss J, Farnam Y. Freeze-thaw crack determination in cementitious materials using 3D X-ray computed tomography and acoustic emission. Cem Concr Compos. 2018;89:120–9.
- 52. Landis EN, Keane DT. X-ray microtomography. Mater Charact. 2010;61:1305–16.
- 53. Provis JL, Myers RJ, White CE, Rose V, Van Deventer JSJ. X-ray microtomography shows pore structure and tortuosity in alkali-activated binders. Cem Concr Res. 2012;42:855–64.
- Dragonfly. 3D visualization and analysis solutions for scientific and industrial data. ORS; 2018. https://www.theobjects.com/dragonfly/index.html. Accessed March 21, 2020.
- Pacheco-Torgal F, Labrincha J, Leonelli C, Palomo A, Chindaprasit
 P. Handbook of alkali-activated cements, mortars and concretes.
 Amsterdam: Elsevier; 2014.
- Song WJ, Tang LH, Zhu XD, Wu YQ, Zhu ZB, Koyama S. Effect of coal ash composition on ash fusion temperatures. Energy Fuels. 2009;24:182–9.
- Mohebbi M, Rajabipour F, Scheetz BE. Reliability of loss on ignition (LOI) test for determining the unburned carbon content in fly ash. World Coal Ash Conf. (WOCA), Nashville, TN, May 2015, p. 5–7
- Fan M, Brown RC. Comparison of the loss-on-ignition and thermogravimetric analysis techniques in measuring unburned carbon in coal fly ash. Energy Fuels. 2001;15:1414–7.
- ASTM C618–19. Standard specification for coal fly ash and raw or calcined natural pozzolan for use in concrete. West Conshohocken, PA, USA ASTM Int. 2019.
- Lee NK, Koh KT, An GH, Ryu GS. Influence of binder composition on the gel structure in alkali activated fly ash/slag pastes exposed to elevated temperatures. Ceram Int. 2017;43:2471–80.
- 61. White CE, Provis JL, Llobet A, Proffen T, Van Deventer JSJ. Evolution of local structure in geopolymer gels: an in situ neutron pair distribution function analysis. J Am Ceram Soc. 2011;94:3532–9.
- Scrivener K, Snellings R, Lothenbach B. A practical guide to microstructural analysis of cementitious materials. Boca Raton: CRC Press; 2018.
- Martin ST. Phase transitions of aqueous atmospheric particles. Chem Rev. 2000;100:3403–54.
- 64. Biskos G, Malinowski A, Russell LM, Buseck PR, Martin ST. Nanosize effect on the deliquescence and the efflorescence of sodium chloride particles. Aerosol Sci Technol. 2006;40:97–106.
- Cong X, Kirkpatrick RJ. Effects of the temperature and relative humidity on the structure of C–S–H gel. Cem Concr Res. 1995;25:1237–45.
- 66. Park SM, Jang JG, Lee NK, Lee H-K. Physicochemical properties of binder gel in alkali-activated fly ash/slag exposed to high temperatures. Cem Concr Res. 2016;89:72–9.
- 67. Bakharev T. Thermal behaviour of geopolymers prepared using class F fly ash and elevated temperature curing. Cem Concr Res. 2006;36:1134–47.
- Lee KH, Lee JH, Wie YM, Lee KG. Bloating mechanism of lightweight aggregates due to ramping rate. Adv Mater Sci Eng. 2019;2019:1–12.
- German RM. Liquid phase sintering. Berlin: Springer Science & Business Media; 2013.
- Bernhardt M, Justnes H, Tellesbø H, Wiik K. The effect of additives on the properties of lightweight aggregates produced from clay. Cem Concr Compos. 2014;53:233–8.

- 71. Carter CB, Norton MG. Ceramic materials: science and engineering, vol. 716. Berlin: Springer; 2007.
- Schonhorn H. Surface tension-viscosity relationship for liquids. J Chem Eng Data. 1967;12:524–5.
- Sparks RSJ. The dynamics of bubble formation and growth in magmas: a review and analysis. J Volcanol Geotherm Res. 1978;3:1–37.
- 74. Yan Z, Wang Z, Liu H, Tu Y, Yang W, Zeng H, et al. Decomposition and solid reactions of calcium sulfate doped with SiO2, Fe2O3 and Al2O3. J Anal Appl Pyrolysis. 2015;113:491–8.
- Swift WM, Panek AF, Smith GW, Vogel GJ, Jonke AA.
 Decomposition of calcium sulfate: a review of the literature.
 Argonne, IL: Argonne National Lab (ANL). 1976.
- 76. Lee KG. Bloating mechanism of lightweight aggregate with the size. J Korean Ceram Soc. 2016;53:241–5.
- 77. Toyama S, Kawamura M. On the relationship between the bloating of lightweight aggregate and reaction progress of the constituents. J Chem Eng Japan. 1971;4:251–6.
- Franus M, Barnat-Hunek D, Wdowin M. Utilization of sewage sludge in the manufacture of lightweight aggregate. Environ Monit Assess. 2016;188:10.
- Luo Y, Zheng S, Ma S, Liu C, Wang X. Preparation of sintered foamed ceramics derived entirely from coal fly ash. Constr Build Mater. 2018;163:529–38.

- 80. Bethanis S, Cheeseman CR, Sollars CJ. Effect of sintering temperature on the properties and leaching of incinerator bottom ash. Waste Manag Res. 2004;22:255–64.
- 81. Verbinnen B, Billen P, Van Caneghem J, Vandecasteele C. Recycling of MSWI bottom ash: a review of chemical barriers, engineering applications and treatment technologies. Waste Biomass Valori. 2017;8:1453–66.

SUPPORTING INFORMATION

Additional supporting information may be found online in the Supporting Information section.

How to cite this article: Balapour M, Rao R, Garboczi EJ, et al. Thermochemical principles of the production of lightweight aggregates from waste coal bottom ash. *J Am Ceram Soc.* 2020;00:1–22. https://doi.org/10.1111/jace.17458

NOMENCLATURE FOR CHEMICAL COMPOUNDS

Chemical formula
TiO ₂
$Ca_3Fe_2Si_3O_{12}$
CaSO ₄
CaAl ₂ Si ₂ O ₈
$(Ca,Na)(Mg,Fe,Al,Ti)(Si,Al)_2O_6$
$Mg(OH)_2$
CaCO ₃
CaMgSi ₂ O ₆
$Na_2Ca_2Si_3O_9$
$Mg_2Al_4Si_5O_{18}$
CaMg(CO ₃) ₂
NaAlSi ₃ O ₈
$CaAl_2Si_2O_8$
Ca ₂ Al ₂ SiO ₇

Name	Chemical formula
Gypsum	CaSO ₄ .2H ₂ O
Hematite	Fe ₂ O ₃
Melilite	$Ca_2Mg(Si_2O_7)$
Merwinite	$Ca_3Mg(SiO_4)_2$
Mullite	$3Al_2O_3.2SiO_2$
Nepheline	NaAlSiO ₄
Orthopyroxene	$\mathrm{Mg_2Si_2O_6}$
Portlandite	Ca(OH) ₂
Rankinite	Ca ₃ Si ₂ O ₇
Tridymite	SiO_2
Wollastonite	CaSiO ₃
C: CaO, A: Al ₂ O ₃ , N: Na ₂ O, S: SiO ₂ , H: H ₂ O	C-A-(N)-S-H
N: Na ₂ O, A: Al ₂ O ₃ , S: SiO ₂ , H: H ₂ O	N-A-S-H
C: CaO, S: SiO ₂ , H: H ₂ O	C-S-H